Supplementary Material

Construction of Alkyl-Substituted Pentaphosphido Ligands in the Coordination Sphere of Cobalt

Christoph G. P. Ziegler,[a] Thomas M. Maier,[a] Stefan Pelties,[a] Clemens Taube,[b] Felix Hennersdorf,[b] Andreas W. Ehlers,[c] Jan J. Weigand,*[b] and Robert Wolf*[a]

Abstract: Rare mono- and diorganopentaphosphido cobalt complexes are accessible by P–P condensation using the unprecedented, reactive cobalt-gallium tetraphosphido complex [K(dme)$_2${(^{Mes}BIAN)Co(μ-η^4:η^2-P$_4$)Ga(nacnac)}] (**2**). Compound **2** was prepared in good yield by reaction of [K(Et$_2$O){(^{Mes}BIAN)Co(η^4-1,5-cod)}] [**1**, BIAN = bis(mesitylimino)acenaphthene diimine, cod = 1,5-cyclooctadiene] with [Ga(nacnac)(η^2-P$_4$)] (nacnac = CH[CMeN(2,6-*i*Pr$_2$C$_6$H$_3$)]$_2$]). Reactions with R$_2$PCl (R = *i*Pr, *t*Bu, and Cy) selectively afford [(^{Mes}BIAN)Co(*cyclo*-P$_5$R$_2$)] (**3a**-**c**), which feature η^4-coordinated 1,1-diorganopentaphosphido ligands. The mechanism of formation of these species has been studied by ^{31}P{^{1}H} NMR spectroscopy and DFT calculations. In case of **3a** (R = *i*Pr), it was possible to identify the intermediate [(^{Mes}BIAN)Co(μ-η^4:η^2-P$_5$*i*Pr$_2$)Ga(nacnac)}] (**4**) by single-crystal X-ray diffraction. A related, monosubstitued organopentaphosphido cobalt complex [(^{Mes}BIAN)Co(μ-η^4:η^1-P$_5$*t*Bu)GaCl(nacnac)] (**5**) was isolated by reacting dichloroalkylphosphane *t*BuPCl$_2$ with **2**. Heterobimetallic complexes such as **2** thus may enable the targeted construction of a range of new metal-coordinated polyphosphorus frameworks by P–P condensation.

C. G. P. Ziegler, T. M. Maier, Dr. S. Pelties, Prof. R. Wolf

University of Regensburg

Institute of Inorganic Chemistry

93040 Regensburg (Germany)

E-mail: *robert.wolf@ur.de*

C. Taube, Dr. F. Hennersdorf, Prof. J. J. Weigand

TU Dresden

Faculty of Chemistry and Food Chemistry, Chair of Molecular Inorganic Chemistry

01062 Dresden (Germany)

E-mail: *jan.weigand@tu-dresden.de*

Dr. A. W. Ehlers

University of Amsterdam

Faculty of Science, van 't Hoff Institute for Molecular Sciences

Science Park 904, 1090 GS Amsterdam (The Netherlands)

University of Johannesburg, Department of Chemistry,

Auckland Park, Johannesburg, 2006, South Africa

Table of Contents

Experimental Procedures

General Remarks

All manipulations were performed under an atmosphere of dry argon using standard Schlenk techniques or an MBraun UniLab glovebox.

Chemicals and Solvents: Solvents were dried and degassed with an MBraun SPS800 solvent-purification system. THF, diehtylether, and toluene were stored over molecular sieves (3 Å). *n*-Hexane was stored over a potassium mirror. 1,2-dimethoxyethane was stirred over K/benzophenone, distilled and stored over molecular sieves (3 Å). *n*-Pentane was stirred over sodium, distilled and stored over a potassium mirror.

NMR spectroscopy: NMR spectra were recorded on Bruker Avance 300 and Avance 400 spectrometers at 300 K and internally referenced to residual solvent resonances (δTMS = 0.00 ppm,^{1}H,^{13}C; δH_3PO_4(85%) = 0.00 ppm, ^{31}P, externally). Chemical shifts (δ) are reported in ppm. Coupling constants (*J*) are reported in Hz. For compounds, which give rise to a higher order spin system in the ^{31}P{^{1}H} NMR spectrum, the resolution enhanced ^{31}P{^{1}H} NMR spectrum was transferred to the software gNMR, version 5.0, by Cherwell Scientific[1]. The full line shape iteration procedure of gNMR was applied to obtain the best match of the fitted to the experimental spectrum. $^{1}J(^{31}P^{31}P)$ coupling constants were set to negative values and all other signs of the coupling constants were obtained accordingly.[2] Assigned atoms in the ^{13}C spectra were indirectly deduced from the cross-peaks in 2D correlation experiments (HMBC, HSQC). ^{31}P NMR reaction monitoring was performed on a Bruker AVANCE III HDX, 500 MHz Ascend (^{31}P(202.45 MHz)). PH-HMBC NMR spectra of compound **5** were recorded on a Bruker Avance III 600 spectrometer with a 5 mm TBI-F probe. ^{1}H chemical shifts were referenced to the THF-d_8 signal at 3.58 ppm. The heteronuclei ^{31}P was referenced, employing $n(X) = n(\text{THF-}d_8) \cdot X_{\text{reference}} / 100$ % according to Harris et al.[3] The following frequency ratio and reference compound was used: $X(^{31}P) = 40.480742$ (H_3PO_4).

Elemental analyses: Elemental analyses were determined by the analytical department of the University of Regensburg with a Micro Vario Cube (Elementar).

UV/vis spectra: UV/vis spectra were recorded on an Ocean Optics Flame spectrometer.

Melting points: Melting points were measured on samples in sealed capillaries on a Stuart SMP10 melting point apparatus.

Chemicals: The starting materials $[K(thf)_{0.2}\{Co(\eta^4\text{-}1,5\text{-}cod)_2\}]$[4], $[K(thf)_{1.5}\{Co(^{Dipp}BIAN)(\eta^4\text{-}1,5\text{-}cod)\}]$[5], $[(nacnac)Ga(\eta^2\text{-}P_4)]$[6] and ^{Mes}BIAN[7] were prepared according to previously reported procedures. *i*Pr_2PCl was purchased from Sigma-Aldrich and used as delivered. Cy_2PCl[8], *t*Bu_2PCl[9], *t*$BuPCl_2$[10] were prepared according to literature procedures.

Synthesis of [K(Et₂O){Co(^Mes BIAN)(η⁴-1,5-cod)}] (1)

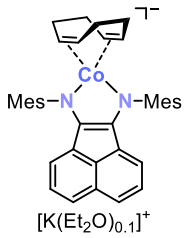

An orange THF solution (20 mL) of ^Mes BIAN (839 mg, 2.0 mmol, 1.0 equiv.) was added to a yellow THF solution (10 mL) of [K(thf)$_{0.2}${Co(η⁴-1,5-cod)$_2$}] (663 mg, 2.02 mmol, 1.0 equiv.). The reaction mixture was stirred at room temperature for 6 h, whereupon the color changed to green. Volatiles were removed in *vacuo* and the remaining green solid was extracted with 200 mL diethylether and filtered through a glass frit. Dark green needles were obtained from the concentrated filtrate after 3 days at room temperature. According the ^{1}H NMR spectroscopy, the isolated sample still contained 0.1 equiv of diethyl ether after drying under vacuum (10^{-3} mbar). Crystals suitable for single X-ray diffraction were obtained by diffusion of *n*-hexane into a concentrated DME solution of [K(dme)$_4${Co(^Mes BIAN)(η⁴-1,5-cod)}] (**1-dme**).

Yield: 558 mg (44%); m.p. >250 °C (decomposition to a black oil); UV/vis: (THF, λ_{max} / nm, ε_{max} / L·mol^{-1}·cm^{-1}): 303 (20000), 442 (10500), 642 (6500). ^{1}H NMR (400.13 MHz, 300 K, THF-d_8): δ / ppm = 6.81 (s, 4H, *m*-CH$_{(Mes)}$), 6.40 (br, m, 2H, CH$_{(BIAN)}$), 6.35 (br, m, 2H, CH$_{(BIAN)}$), 5.21 (d, $^3J_{HH}$ = 6.0 Hz, 2H, CH$_{(BIAN)}$), 3.64 (br, THF), 2.67 (s, 4H, CH$_{(cod)}$), 2.46 (s, 12H, *o*-CH$_{3(Mes)}$), 2.34 (s, 4H, CH$_{2(cod)}$), 2.25 (s, 6H, *p*-C*H*$_{3(Mes)}$), 1.78 (br, THF), 1.01 (br m, 4H, CH$_{2(cod)}$); ^{13}C{^{1}H} (100.61 MHz, 300 K, THF-d_8): δ / ppm = 153.0 (*ipso*-C$_{Mes}$), 137.2 (C$_{BIAN}$), 134.4 (C$_{BIAN}$), 130.5 (C$_{Mes}$), 128.6 (CH$_{Mes}$), 127.8 (CH$_{BIAN}$), 127.3 (C$_{Mes}$) 119.2 (CH$_{BIAN}$), 112.6 (CH$_{BIAN}$), 65.6 (cod-CH), 32.5 (cod-CH$_2$), 21.2 (*p*-CH$_{3(Mes)}$), 19.3 (*o*-CH$_{3(Mes)}$), resonances of two quaternary carbon atoms were not detected; elemental analysis calcd. for $C_{38}H_{40}CoKN_2 \cdot (C_4H_{10}O)_{0.x}$ (x = 1-4) Mw = 630.20 g·mol^{-1}): C 73.19, H 6.56, N 4.45; found C 72.58, H 6.32; N 4.34; the deviation in the carbon content is explained by a varying amount of solvate molecules present in isolated sample of **1**.

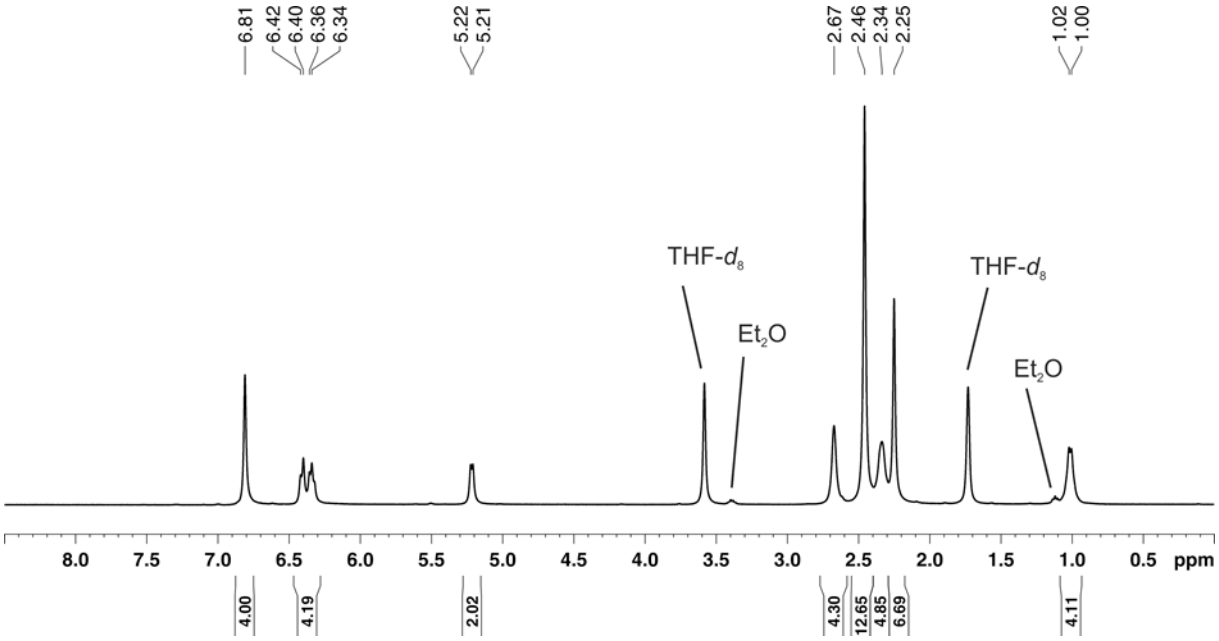

Figure S1. ^{1}H NMR spectrum (400.13 MHz, 300 K, THF-d_8) of [K(Et$_2$O){Co(^Mes BIAN)(η⁴-1,5-cod)}] (**1**).

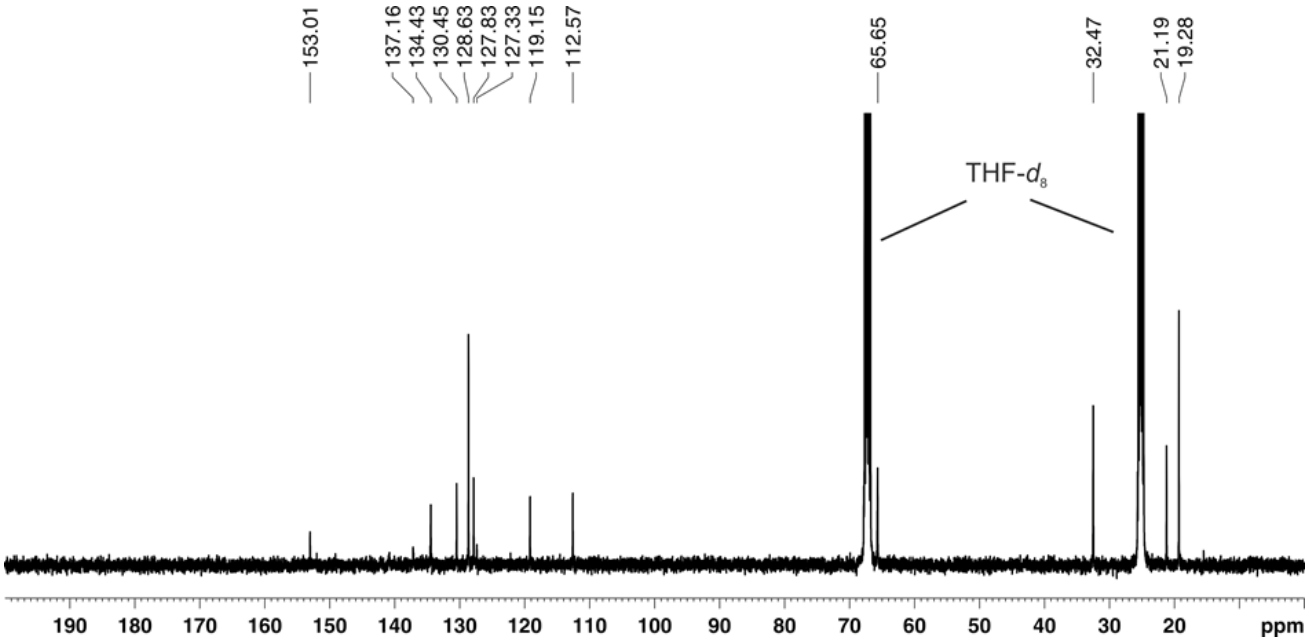

Figure S2. $^{13}C\{^1H\}$ NMR spectrum (100.61 MHz, 300 K, THF-d_8) of [K(Et$_2$O){Co(^{Mes}BIAN)(η^4-1,5-cod)}] (**1**).

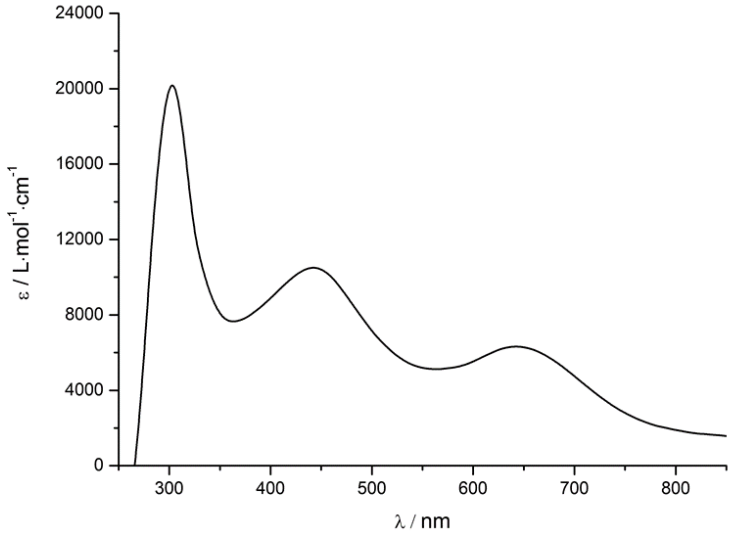

Figure S3. UV/vis spectrum of [K(Et$_2$O){Co(^{Mes}BIAN)(η^4-1,5-cod)}] (**1**) recorded in THF.

Synthesis of [K(dme)$_2${(^{Mes}BIAN)Co(μ-η^4:η^2-P$_4$)Ga(nacnac)}] (2)

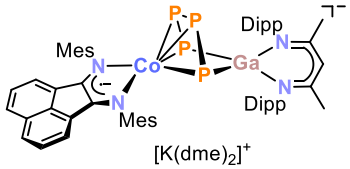

A green THF solution (15 mL) of [K(Et$_2$O)$_{0.1}${Co(^{Mes}BIAN)(1,5-cod)}] (**1**) (479 mg, 0.761 mmol, 1.0 equiv.) was added to a yellow THF solution (25 mL) of [(nacnac)Ga(η^2-P$_4$)] (500 mg, 0.761 mmol, 1.0 equiv.). The resulting green reaction mixture turned dark violet upon vigorous stirring for 3 days at room temperature. Volatiles were removed in *vacuo* and the remaining violet solid was washed with 20 mL *n*-hexane. The crude product was redissolved in 30 mL DME, filtered through a glass frit and concentrated. Dark violet needles were obtained by layering the DME solution with *n*-hexane (1:2) after storage for 3 days at room temperature. The isolated product contains 2 DME molecules and 0.1 *n*-hexane solvate molecules per formula unit after drying in *vacuo* (10^{-3} mbar) according to the ^{1}H NMR spectrum.

Yield: 566 mg (59%); m.p. >250 °C (decomposition to black oil); UV/vis: (THF, λ_{max} / nm, ε_{max} / L·mol^{-1}·cm^{-1}): 321 (44500), 400 (16000), 553(21000), 658 (21000); ^{1}H NMR (400.13 MHz, 300 K, THF-d_8): δ / ppm = 7.37 (m, 1H, CH$_{Dipp}$), 7.28 (d, *J* = 7.4 Hz, 2H, CH$_{Dipp}$), 7.03 (m, 1H, CH$_{Dipp}$), 6.95 (d, $^3J_{HH}$ = 7.4 Hz, 2H, CH$_{Dipp}$), 6.73 (s, 4H, CH$_{Mes}$), 6.54 (dd, $^3J_{HH}$ = 7.1 Hz, 8.0 Hz, 2H, CH$_{BIAN}$), 5.43 (d, $^3J_{HH}$ = 7.0 Hz, 2H, CH$_{BIAN}$), 4.70 (s, 1H, CH$_{nacnac}$), 3.78 (sept, $^3J_{HH}$ = 6.8 Hz, 2H, C*H*(CH$_3$)$_2$), 3.43 (s, DME), 3.28 (s, DME), 2.73 (sept, $^3J_{HH}$ = 6.8 Hz, 2H, C*H*(CH$_3$)$_2$), 2.34 (s, 6H, *p*-CH$_{3(Mes)}$), 1.87 (s, 12H, *o*-CH$_{3(Mes)}$), 1.54 (s, 3H, CH$_{3(nacnac)}$), 1.48 (d, $^3J_{HH}$ = 6.8 Hz, 6H, CH(C*H*$_3$)$_2$), 1.42 (s, 3H, CH$_{3(nacnac)}$), 1.37 (d, $^3J_{HH}$ = 6.8 Hz, 6H, CH(C*H*$_3$)$_2$), 1.18 (d, $^3J_{HH}$ = 6.8 Hz, 6H, CH(C*H*$_3$)$_2$), 0.86 (d,

$^{3}J_{HH}$ = 6.8 Hz, 6H, CH(CH_3)$_2$); ^{13}C{^{1}H} (100.61 MHz, 300 K, THF-d_8): δ / ppm = 167.9 (CN_{nacnac}), 165.9 (CN_{nacnac}), 154.9 (C_{Mes}), 147.8 (CN_{BIAN}), 145.2 (CN_{Dipp}), 145.0 (CN_{Dipp}), 143.9 (C_{Dipp}), 143.0 (C_{Dipp}), 137.5 (C_{BIAN}), 135.7 (C_{BIAN}), 132.1 (C_{Mes}), 131.6 (C_{Mes}), 130.8 (C_{BIAN}), 128.7 (CH_{BIAN}), 128.3 (CH_{Mes}), 127.4 (CH_{Dipp}), 126.5 (CH_{Dipp}), 125.2 (CH_{Dipp}), 124.4 (CH_{Dipp}), 121.5 (CH_{BIAN}), 115.7 (CH_{BIAN}), 95.8 (CH_{nacnac}), 29.5 (*C*H(CH$_3$)$_2$), 29.0 (*C*H(CH$_3$)$_2$), 26.6 (CH(*C*H$_3$)$_2$), 26.5 (CH(*C*H$_3$)$_2$), 24.6 ($CH_{3(nacnac)}$), 24.5($CH_{3(nacnac)}$), 21.3 (*p*-$CH_{3(Mes)}$), 19.6 (*o*-$CH_{3(Mes)}$); ^{31}P{^{1}H} NMR (161.98 MHz, 300 K, THF-d_8): (AA'XX') spin system δ / ppm = 74.0 (m, 2P_P), −125.4 (m, 2P_{Ga}); elemental analysis calcd. for $C_{59}H_{69}CoGaN_4P_4K \cdot (C_4H_{10}O_2)_2 \cdot (C_6H_{14})_{0.1}$ (Mw = 1314.7 g·mol^{-1}): C 61.76, H 6.93, N 4.26; found C 61.66, H 6.69; N 4.35.

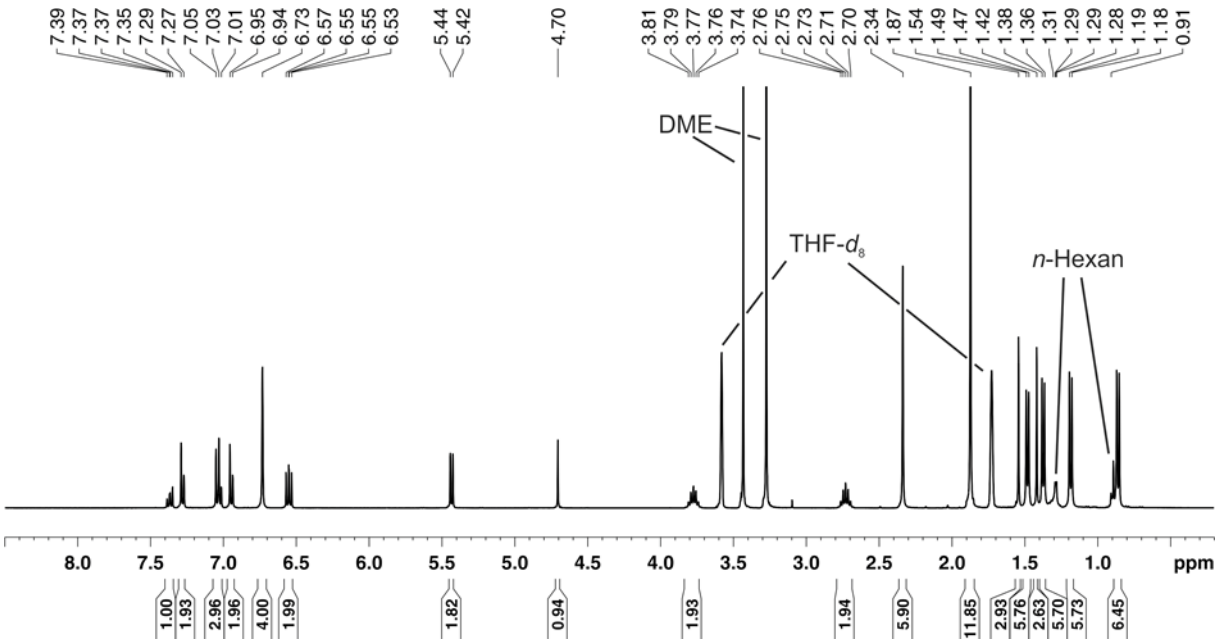

Figure S4. ^{1}H NMR spectrum (400.13 MHz, 300 K, THF-d_8) of [K(dme)$_2${(^{Mes}BIAN)Co(μ-η^4:η^2-P_4)Ga(nacnac)}] (**2**).

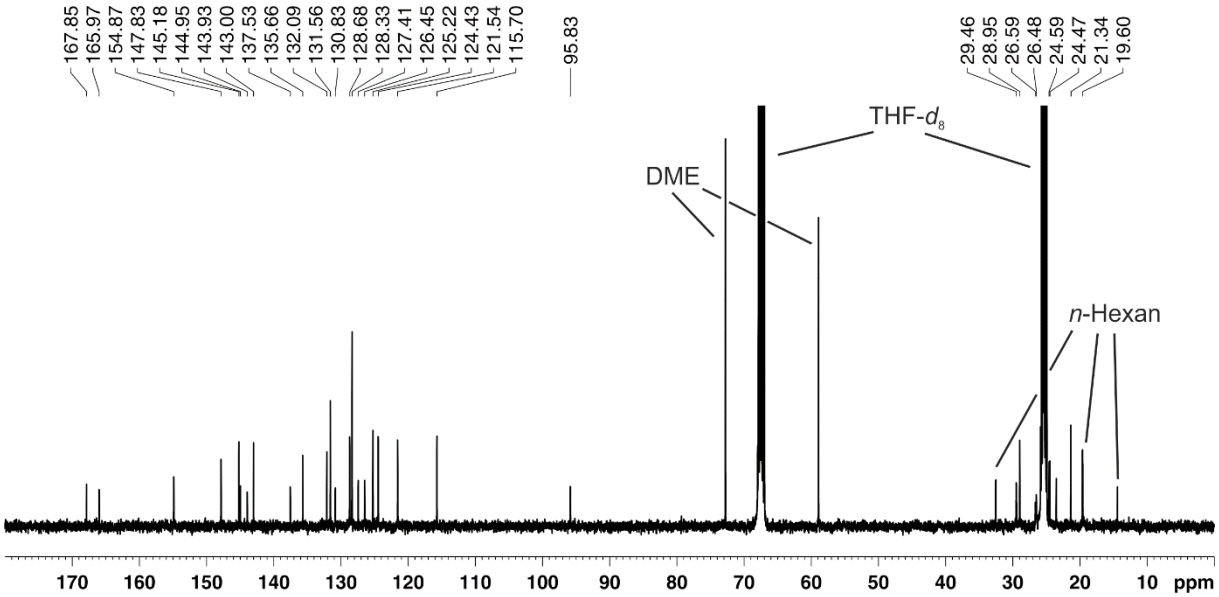

Figure S5. ^{13}C{^{1}H} NMR spectrum (100.61 MHz, 300 K, THF-d_8) of [K(dme)$_2${(^{Mes}BIAN)Co(μ-η^4:η^2-P_4)Ga(nacnac)}] (**2**).

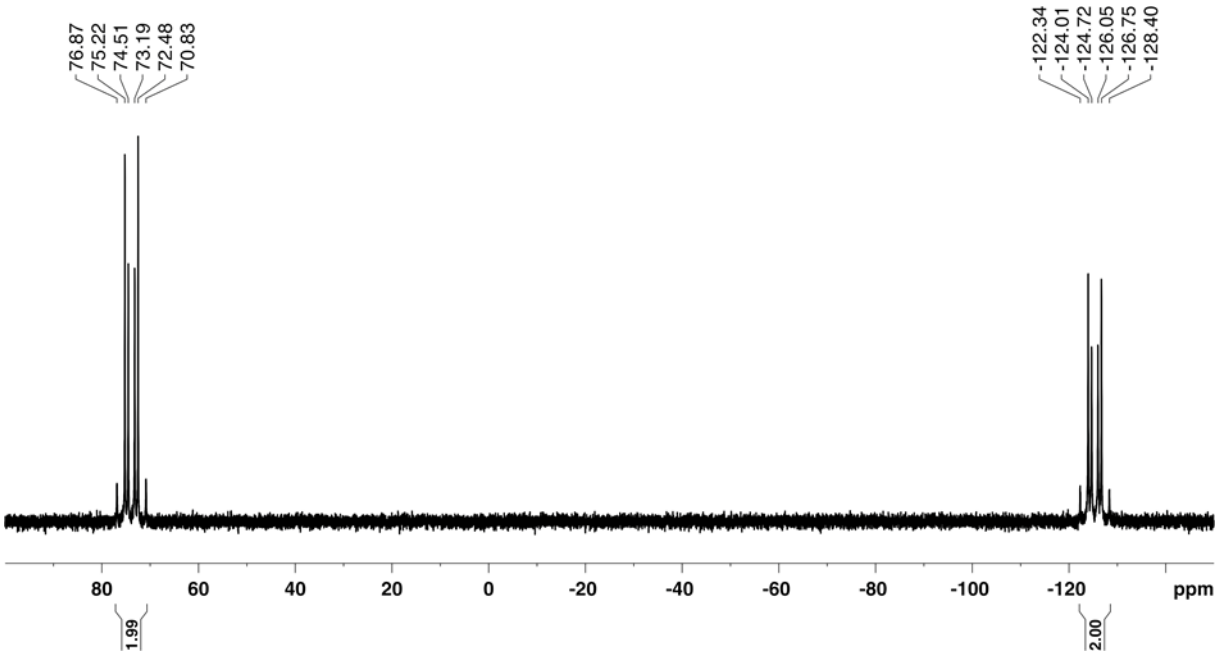

Figure S6. $^{31}P\{^{1}H\}$ NMR spectrum (161.98 MHz, 300 K, THF-d_8) of [K(dme)$_2${(^{Mes}BIAN)Co(μ-η^4:η^2-P$_4$)Ga(nacnac)}] (**2**).

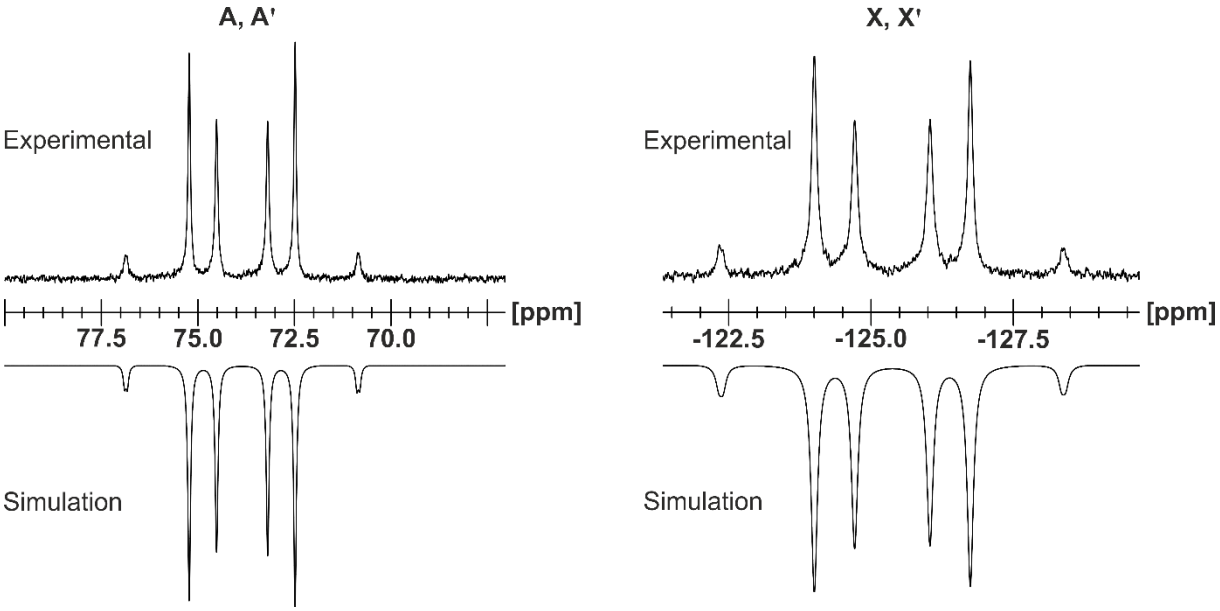

Figure S7. Section of the $^{31}P\{^{1}H\}$ NMR (400.13 MHz, 300 K, THF-d_8) of [K(dme)$_2${(^{Mes}BIAN)Co(μ-η^4:η^2-P$_4$)Ga(nacnac)}] (**2**); experimental (upwards) and simulation (downwards).

Table S1. Coupling constants from the iterative fit of the AA'XX' spin system and schematic representation of the CoP$_4$Ga core of [K(dme)$_2${(^{Mes}BIAN)Co(μ-η^4:η^2-P$_4$)Ga(nacnac)}] (**2**); [Co] = (^{Mes}BIAN)Co, [Ga] = (nacnac)Ga.

$^1J_{AA'} = {}^1J_{A'A}$	−380.5 Hz	$^2J_{AX'} = {}^2J_{A'X}$	6.6 Hz
$^1J_{AX} = {}^1J_{A'X'}$	−450.5 Hz	$^3J_{XX'} = {}^3J_{X'X}$	−7.2 Hz

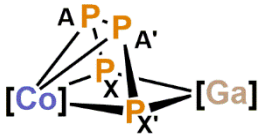

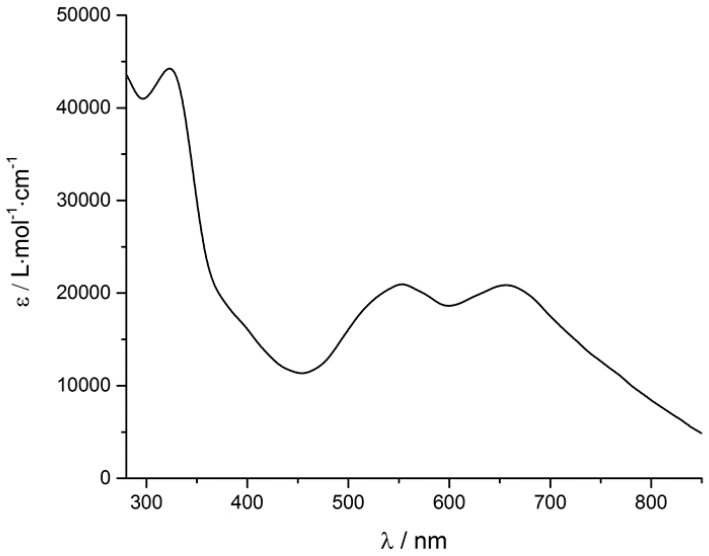

Figure S8. UV/vis spectrum of [K(dme)$_2${(^{Mes}BIAN)Co(μ-η^4:η^2-P$_4$)Ga(nacnac)}] (**2**) recorded in THF.

Synthesis of [K(thf)$_2${(^{Dipp}BIAN)Co(μ-η^4:η^2-P$_4$)Ga(nacnac)}] (2')

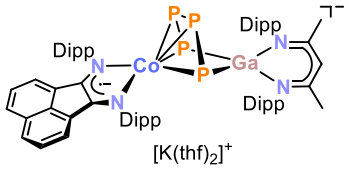

A green THF solution (2 mL) of [K(thf)$_{1.8}${Co(^{Dipp}BIAN)(1,5-cod)}] (72.2 mg, 0.0924 mmol, 1.0 equiv.) was added to a yellow THF solution (2 mL) of [(nacnac)Ga(P$_4$)] (56.5 mg, 0.0924 mmol, 1.0 equiv.). The resulting green reaction mixture turned dark violet upon vigorous stirring for 3 days at room temperature. Volatiles were removed in *vacuo* and the remaining violet solid was extracted with diethylether (5 mL) and filtered. After 2 days dark violet crystals were obtained by slow diffusion of *n*-pentane into a concentrated diethylether solution of the crude product **2'**. The isolated product contains 2 THF molecules per formula unit after drying under vaccuum (10^{-3} mbar) according to the ^{1}H NMR spectrum. Recrystallization by slow diffusion of *n*-hexane into a concentrated solution of **2'** dissolved DME afforded crystals suitable for single crystal X-ray diffraction.

Yield: 66.1 mg (53%); m.p. >250 °C (decomposition to black oil); UV/vis: (THF, λ_{max} / nm, ε_{max} / L·mol^{-1}·cm^{-1}): 332 (32000), 538 (15500), 751 (11500); ^{1}H NMR (400.13 MHz, 300 K, THF-d_8): δ / ppm = 7.15-7.22 (m, 5H, CH$_{Dipp}$), 7.04-7.05 (m, 5H, CH$_{Dipp}$), 6.98 (d, $^3J_{HH}$ = 7.8 Hz, 2H, CH$_{BIAN}$), 6.96 (m, 2H, CH$_{Dipp}$), 6.50 (t, $^3J_{HH}$ = 7.8 Hz, 2H, CH$_{BIAN}$), 5.21 (d, $^3J_{HH}$ = 7.2 Hz, 2H, CH$_{BIAN}$), 4.78 (s, 1H, CH$_{nacnac}$), 3.73 (sept., $^3J_{HH}$ = 6.7 Hz, 2H, C*H*(CH$_3$)$_{2(Dipp)}$), 3.56 (sept., $^3J_{HH}$ = 6.7 Hz, 4H, C*H*(CH$_3$)$_{2(Dipp)}$), 2.75 (sept., $^3J_{HH}$ = 6.7 Hz, 2H, C*H*(CH$_3$)$_{2(Dipp)}$), 1.49 (d, $^3J_{HH}$ = 6.7 Hz, 6H, CH(C*H*$_3$)$_{2(Dipp)}$), 1.47 (s, 3H, CH$_{3(nacnac)}$), 1.42 (s, 3H, CH$_{3(nacnac)}$), 1.38 (d, $^3J_{HH}$ = 6.7 Hz, 6H, CH(C*H*$_3$)$_{2(Dipp)}$), 1.28 (d, $^3J_{HH}$ = 6.7 Hz, 12H, CH(C*H*$_3$)$_{2(Dipp)}$), 1.22 (d, $^3J_{HH}$ = 6.7 Hz, 6H, CH(C*H*$_3$)$_{2(Dipp)}$), 0.57 (d, $^3J_{HH}$ = 6.7 Hz, 6H, CH(C*H*$_3$)$_{2(Dipp)}$), 0.57 (d, $^3J_{HH}$ = 6.7 Hz, 12H, CH(C*H*$_3$)$_{2(Dipp)}$); ^{13}C{^{1}H} (100.61 MHz, 300 K, THF-d_8): δ / ppm = 167.8 (CN$_{nacnac}$), 166.5 (CN$_{nacnac}$), 154.5 (C$_{DippBIAN}$), 149.4 (C$_{BIAN}$), 145.4 (C$_{Dippnacnac}$), 144.4 (C$_{Dippnacnac}$), 143.2 (C$_{DippBIAN}$), 142.9 (C$_{Dippnacnac}$), 137.3 (C$_{BIAN}$), 136.3 (C$_{BIAN}$), 130.4 (C$_{BIAN}$), 127.8 (CH$_{BIAN}$), 127.2 (CH$_{Dipp}$), 126.5 (CH$_{Dippnacnac}$), 124.7 (CH$_{Dippnacnac}$), 124.5 (CH$_{DippBIAN}$), 124.4 (CH$_{Dippnacnac}$), 123.1 (CH$_{DippBIAN}$), 121.6 (CH$_{BIAN}$), 118.0 (CH$_{BIAN}$), 97.0 (*C*H$_{nacnac}$), 29.3 (*C*H(CH$_3$)$_{2(Dipp)}$), 28.9 (*C*H(CH$_3$)$_{2(Dipp)}$), 26.7 (CH(*C*H$_3$)$_{2(Dipp)}$), 25.6 (CH(*C*H$_3$)$_{2(Dipp)}$), 25.5 (CH(*C*H$_3$)$_{2(Dipp)}$), 25.2 (CH(*C*H$_3$)$_{2(Dipp)}$), 25.1 (CH(*C*H$_3$)$_{2(Dipp)}$), 25.0 (CH(*C*H$_3$)$_{2(Dipp)}$), 24.9 (CH$_{3(nacnac)}$), 24.7 (CH$_{3(nacnac)}$); ^{31}P{^{1}H} NMR (161.98 MHz, 300 K, THF-d_8): (AA'XX') spin system δ / ppm = 79.1 (m, 2P$_P$), −133.3 (m, 2P$_{Ga}$); Elemental analysis calcd. for $C_{73}H_{97}N_4CoGaKO_2P_4$ (Mw = 1354.25 g·mol^{-1}): C 64.74, H 7.22, N 4.14; found C 63.85, H 6.76, N 4.05; the carbon content deviates from the calculated values; this may partly be explained by a varying amount of solvate molecules present in isolated sample of **1**, but the complete reasons for this deviations are presently unclear.

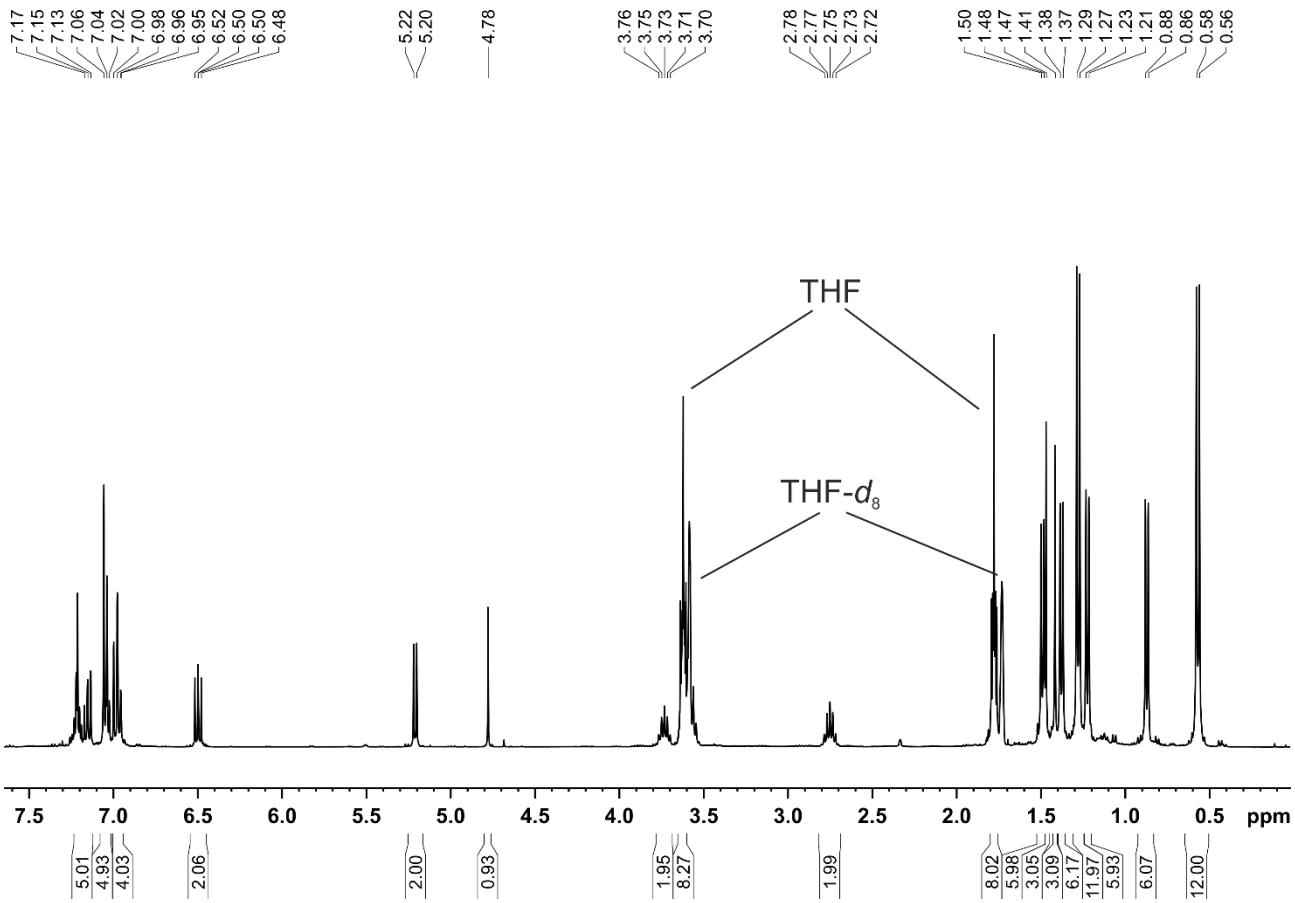

Figure S9. ^{1}H NMR spectrum (400.13 MHz, 300 K, THF-d_8) of [K(thf)$_2${(^{Dipp}BIAN)Co(μ-η^4:η^2-P$_4$)Ga(nacnac)}] (**2'**).

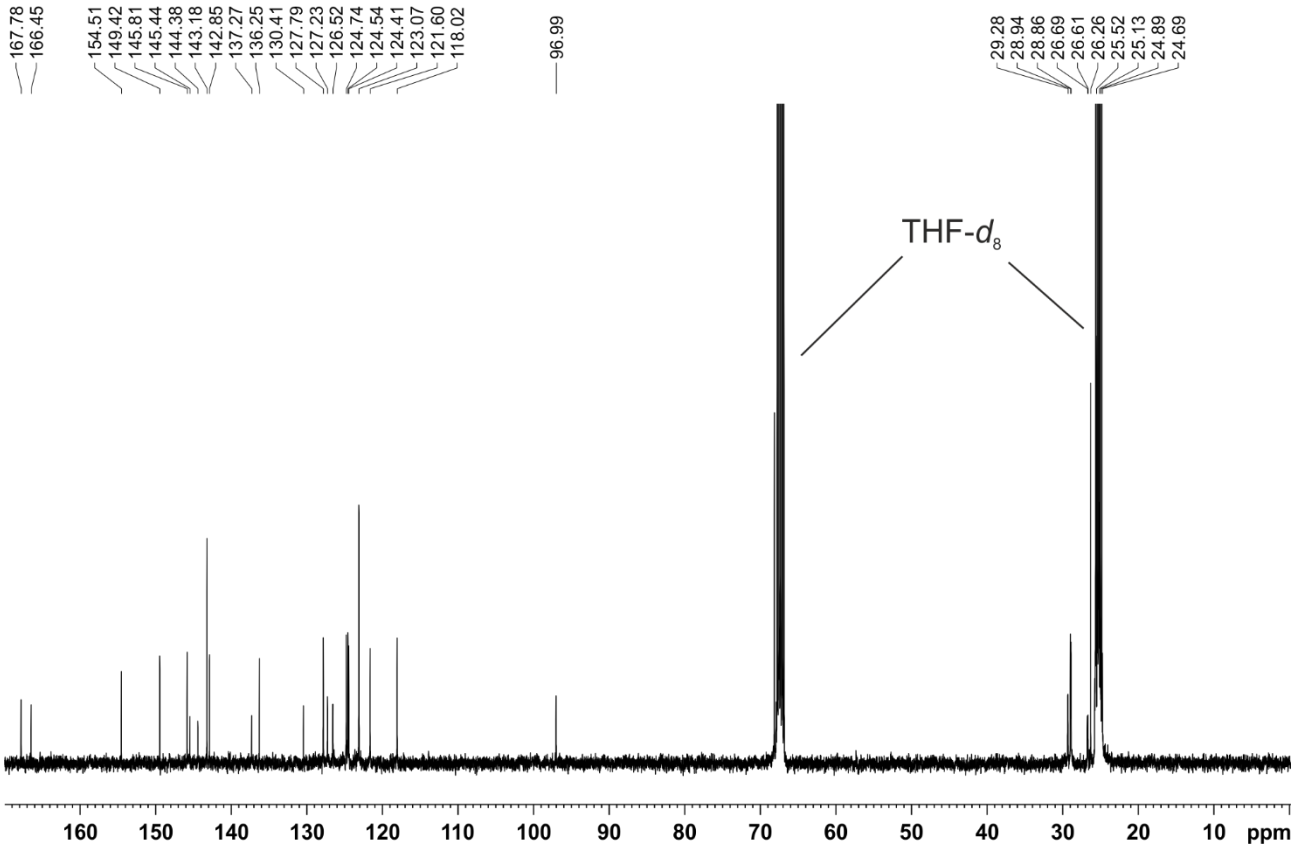

Figure S10. ^{13}C{^{1}H} NMR spectrum (100.61 MHz, 300 K, THF-d_8) of [K(thf)$_2${(^{Dipp}BIAN)Co(μ-η^4:η^2-P$_4$)Ga(nacnac)}] (**2'**).

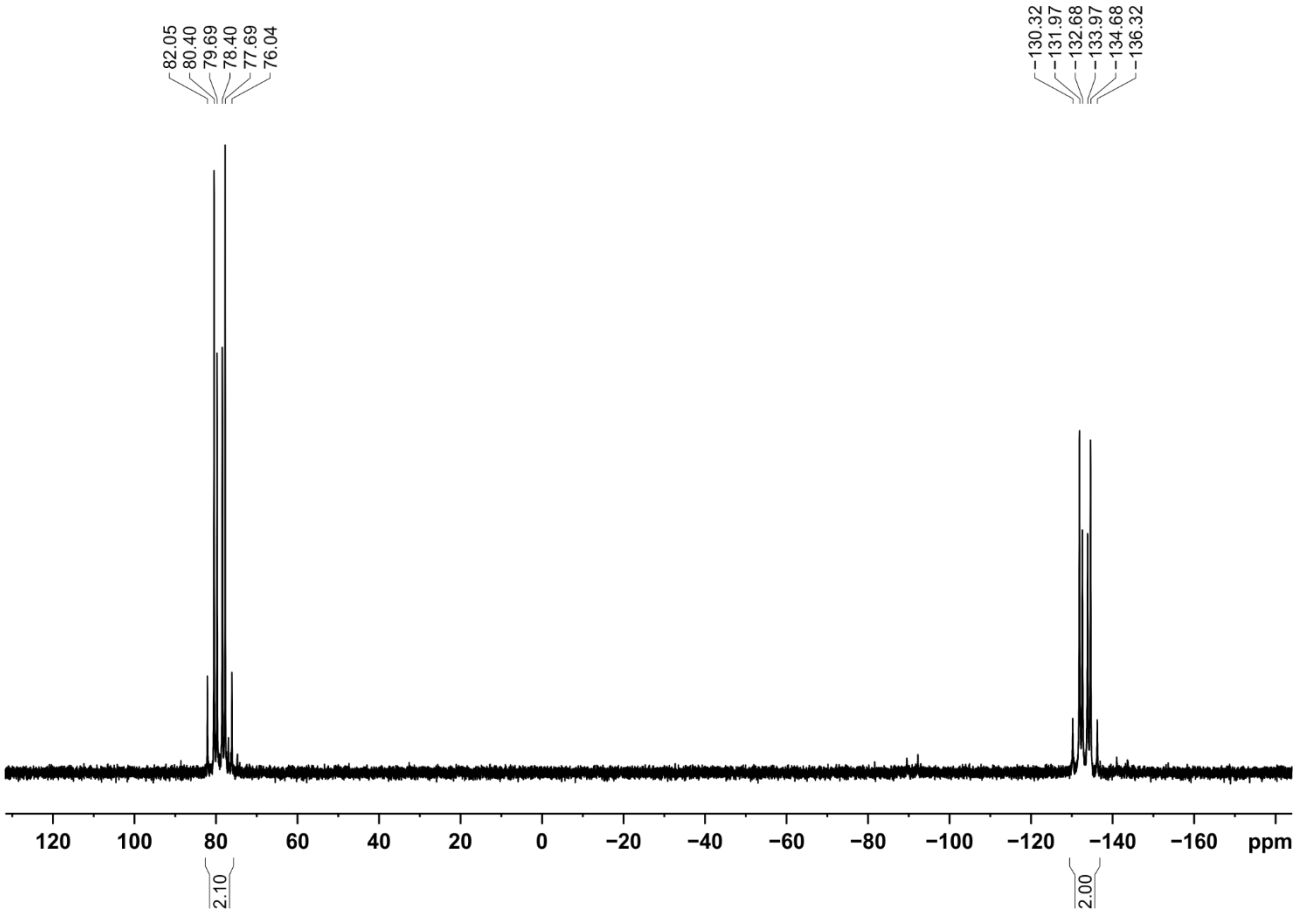

Figure S11. $^{31}P\{^{1}H\}$ NMR spectrum (161.98 MHz, 300 K, THF-d_8) of [K(thf)$_2${(^{Dipp}BIAN)Co(μ-η^4:η^2-P$_4$)Ga(nacnac)}] (**2'**).

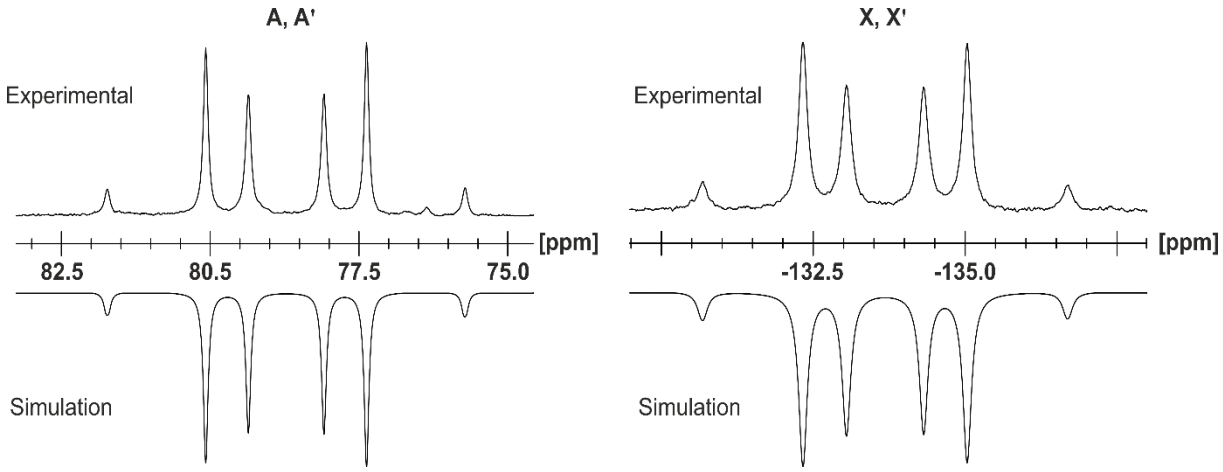

Figure S12. Section of the $^{31}P\{^{1}H\}$ NMR (400.13 MHz, 300 K, THF-d_8) of [K(thf)$_2${(^{Dipp}BIAN)Co(μ-η^4:η^2-P$_4$)Ga(nacnac)}] (**2'**); experimental (upwards) and simulation (downwards).

Table S2. Coupling constants from the iterative fit of the AA'XX' spin and schematic representation of the CoP$_4$Ga core of [K(thf)$_2${(^{Dipp}BIAN)Co(μ-η^4:η^2-P$_4$)Ga(nacnac)}] (**2'**); [Co] = (^{Mes}BIAN)-Co, [Ga] = (nacnac)Ga.

$^1J_{AA'} = {}^1J_{A'A}$	−383.9 Hz	$^2J_{AX'} = {}^2J_{A'X}$	5.0 Hz
$^1J_{AX} = {}^1J_{A'X'}$	−442.7 Hz	$^3J_{XX'} = {}^3J_{X'X}$	−4.8 Hz

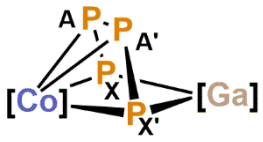

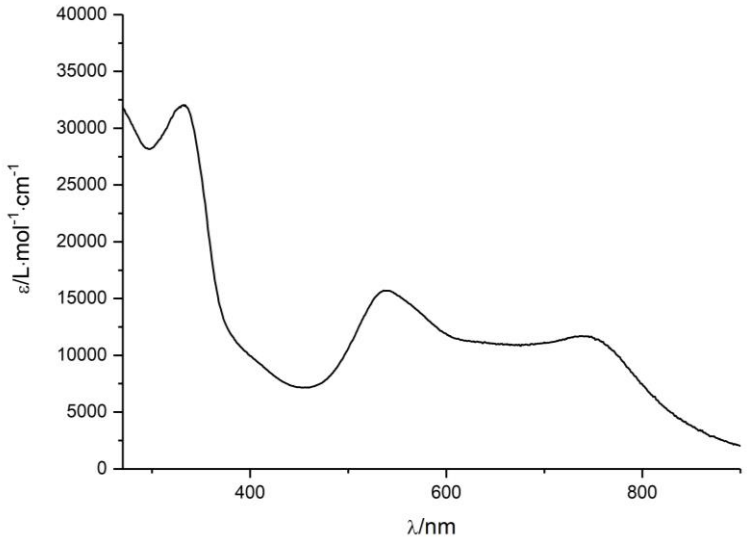

Figure S13. UV/vis spectrum of [K(thf)$_2${(^{Dipp}BIAN)Co(μ-η^4:η^2-P$_4$)Ga(nacnac)}] (**2'**) recorded in THF.

Synthesis of [(^{Mes}BIAN)Co(cyclo-P$_5$*i*Pr$_2$)] (3a)

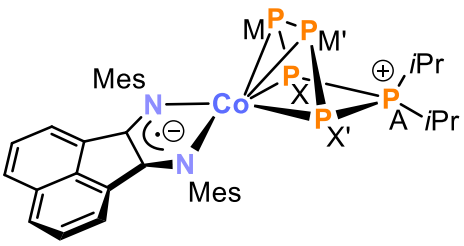

A solution of *i*Pr$_2$PCl in THF (0.91 mL, c = 0.18 mol·L^{-1}, 1.0 equiv.) was added to a dark violet THF solution (10 mL) of [K(dme)$_2${(^{Mes}BIAN)Co(μ-η^4:η^2-P$_4$)Ga(nacnac)}] (**2**) (200 mg, 0.17 mmol, 1.0 equiv.) and stirred at 60 °C for 2 days. A color change of the reaction mixture to cyan was observed. The by-product [Ga(nacnac)] was separated by column chromatography, (stationary phase: neutral aluminum oxide, activity grade: Super I, 10 x 2 cm, eluent: *n*-hexane/toluene gradient, 100/0 to 0/100). [Ga(nacnac)] hydrolyses on aluminum oxide to nacnacH, which elutes first as colorless band (R$_f$ (*n*-hexane/toluene, 7/1 = 0.6). The following blue band (R$_f$ (*n*-hexane/toluene, 7/1 = 0.2) was collected, the obtained solution concentrated in *vacuo* and crystallization by *n*-hexane diffusion gave X-ray quality crystals of **3a** after three days storage at room temperature.

Yield: 32.1 mg (27%); m.p. 248 °C (decomposition to violet oil); UV/vis: (THF, λ$_{max}$ / nm, ε$_{max}$ / L·mol^{-1}·cm^{-1}): 324sh (14500), 332 (15000), 420 (10000), 572 (16000), 578 (16500); ^{1}H NMR (400.13 MHz, 300 K, C$_6$D$_6$): δ / ppm = 7.31 (d, $^3J_{HH}$ =8.2 Hz, 2H, CH$_{(BIAN)}$), 6.95 (s, 4H. *m*-CH$_{(Mes)}$), 6.72 (dd, $^3J_{HH}$ =7.0 Hz, $^3J_{HH}$ =8.2 Hz, 2H, CH$_{(BIAN)}$), 6.54 (d, $^3J_{HH}$ =7.0 Hz, 2H, CH$_{(BIAN)}$), 2.44 (s, 12H, *o*-CH$_{3(Mes)}$) overlap with 2.44 (m, 1H, C*H*(CH$_3$)$_2$), 2.28 (s, 6H, *p*-CH$_{3(Mes)}$), 0.98 (dd, $^3J_{HP}$ = 14.6 Hz, $^3J_{HH}$ = 7.3 Hz, 6H, CH(C*H*$_3$)$_2$), 0.69 (m, 1H, C*H*(CH$_3$)$_2$), 0.22 (dd, $^3J_{HP}$ = 16.0 Hz, $^3J_{HH}$ = 7.1 Hz, 6H, CH(C*H*$_3$)$_2$);^{13}C{^{1}H} NMR (100.61 MHz, 300 K, THF-*d*$_8$): δ / ppm = 154.5 (C$_{(BIAN)}$), 153.2 (C$_{(Mes)}$), 139.4 (C$_{(BIAN)}$), 134.9 (C$_{(Mes)}$), 133.0 (C$_{(BIAN)}$), 131.8 (C$_{(BIAN)}$), 129.5 (C$_{(Mes)}$), 129.4 (*C*H$_{(Mes)}$), 129.0 (*C*H$_{(BIAN)}$), 125.0 (*C*H$_{(BIAN)}$), 118.7 (*C*H$_{(BIAN)}$) 30.1 (br, *C*H(CH)$_2$), 27.6 (br, *C*H(CH)$_2$), 22.1 (br, CH(*C*H$_3$)$_2$), 21.2 (*p*-*C*H$_{3(Mes)}$), 19.4 (*o*-*C*H$_{3(Mes)}$), 17.6 (CH(*C*H$_3$)$_2$); ^{31}P{^{1}H} NMR (161.98 MHz, 300 K, C$_6$D$_6$): (AMM'XX') spin system δ / ppm = 161.0 (m, 1P$_A$), 88.6 (m, 2P$_{MM'}$), −111.4 (m, P$_{XX'}$); elemental analysis calcd. for C$_{36}$H$_{42}$CoN$_2$P$_5$ · (C$_6$H$_{14}$)$_{0.3}$ (Mw = 742.40 g·mol^{-1}): C 61.16, H 6.27, N 3.77; found C 62.57, H 6.58; N 3.54. According to ^{1}H NMR spectroscopy the compound contains 0.3 molecules *n*-hexane per formula unit after drying under vacuum (10^{-3} mbar). Even after two times of recrystallization, the elemental analysis showed a higher C-value than expected for this composition indicating varying concentration of the solvate.

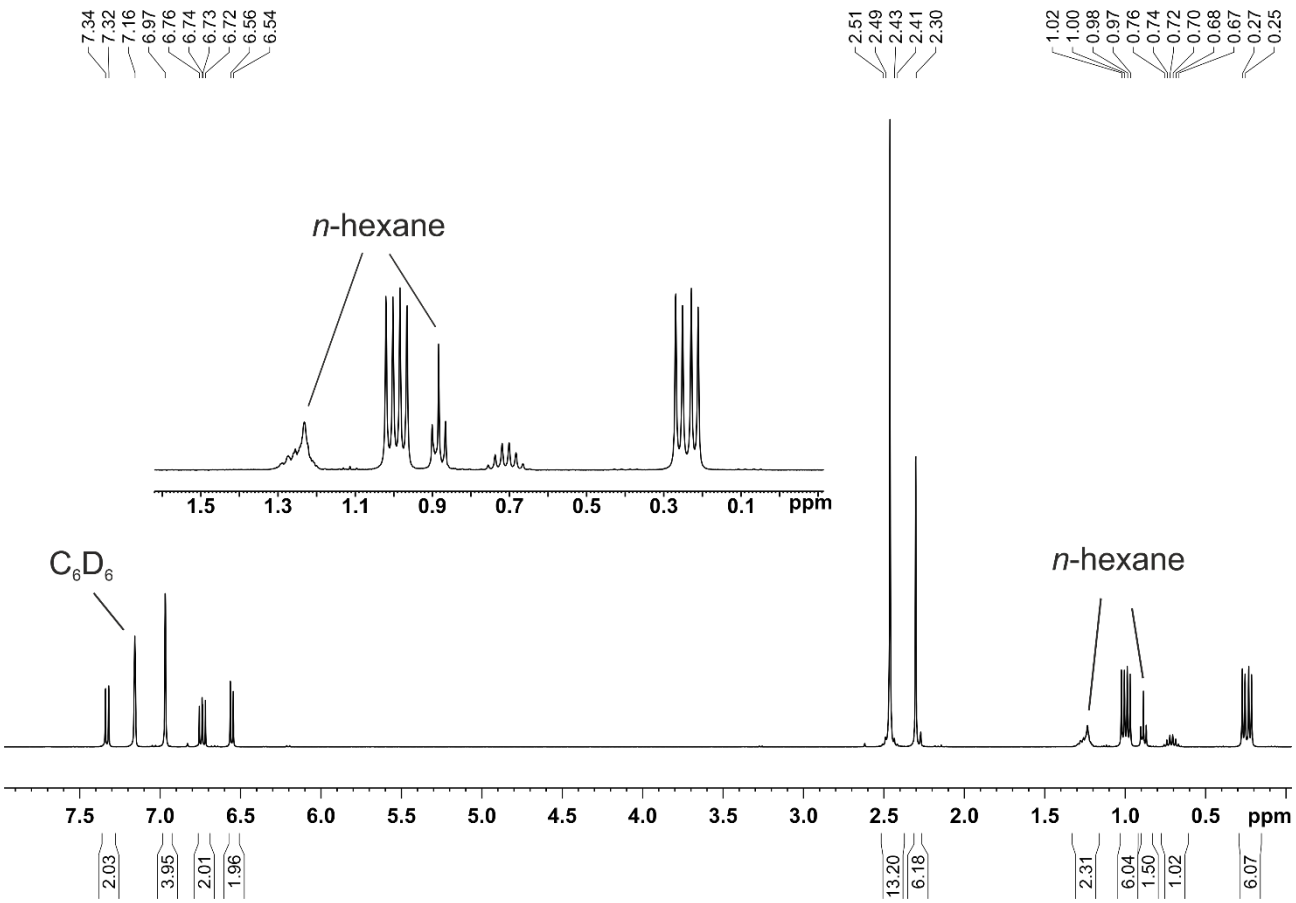

Figure S14. ^{1}H NMR spectrum (400.13 MHz, 300 K, C_6D_6) of [(^{Mes}BIAN)Co(cyclo-P_5iPr$_2$)] (**3a**).

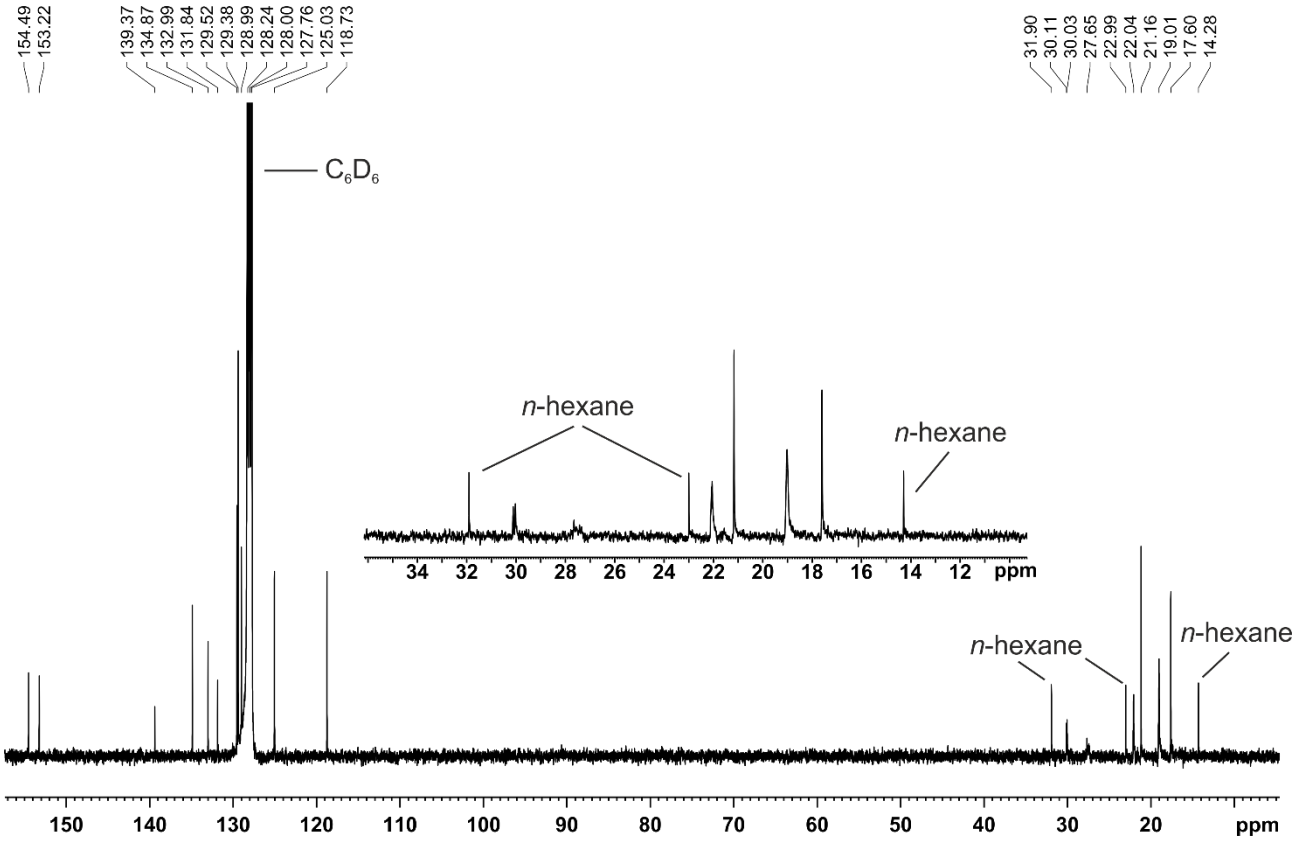

Figure S15. $^{13}C\{^{1}H\}$ NMR spectrum (100.61 MHz, 300 K, C_6D_6) of [(^{Mes}BIAN)Co(cyclo-P_5iPr$_2$)] (**3a**).

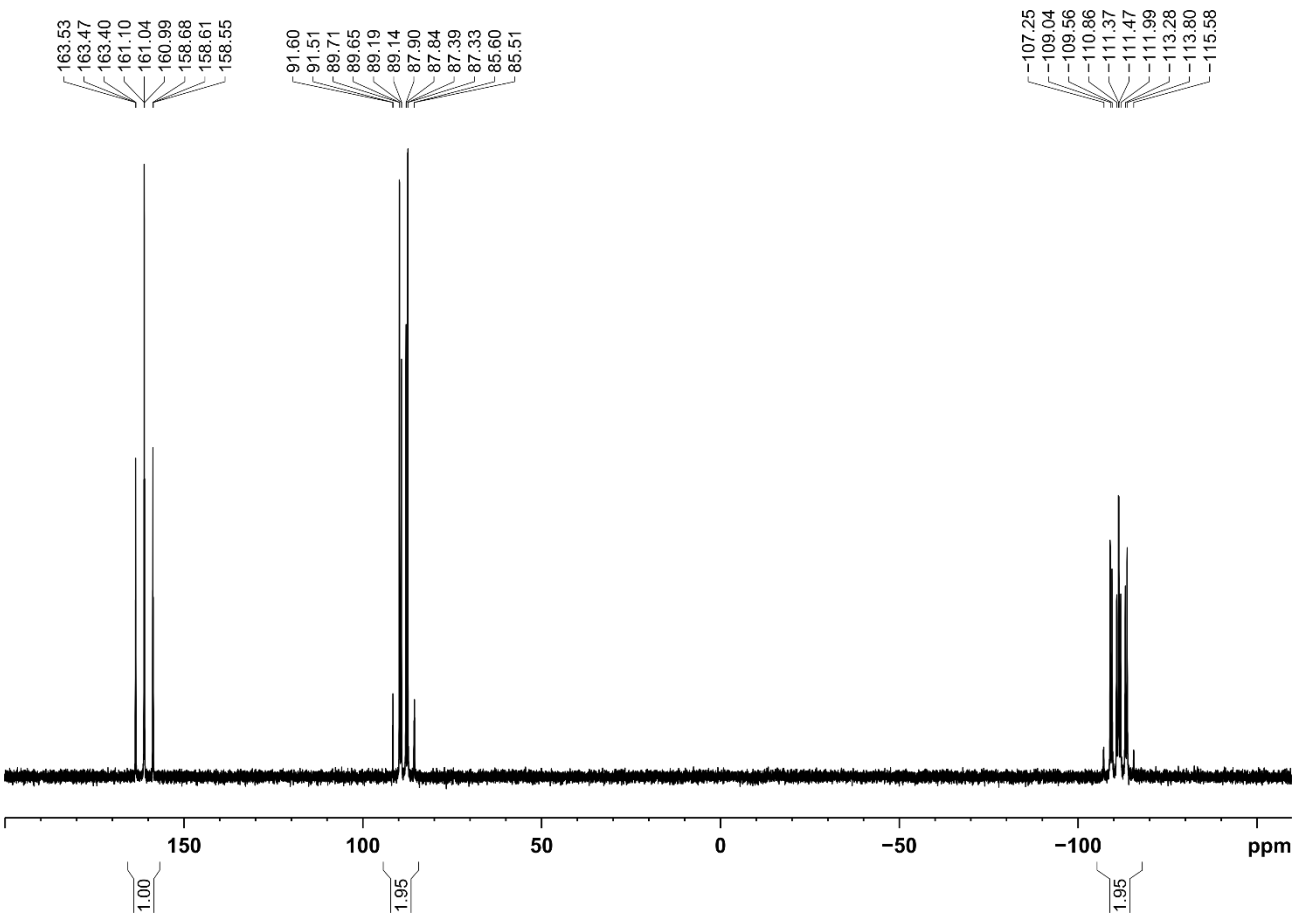

Figure S16. $^{31}P\{^{1}H\}$ NMR spectrum (161.98 MHz, 300 K, C_6D_6) of [(^{Mes}BIAN)Co(cyclo-P_5*i*Pr_2)] (**3a**).

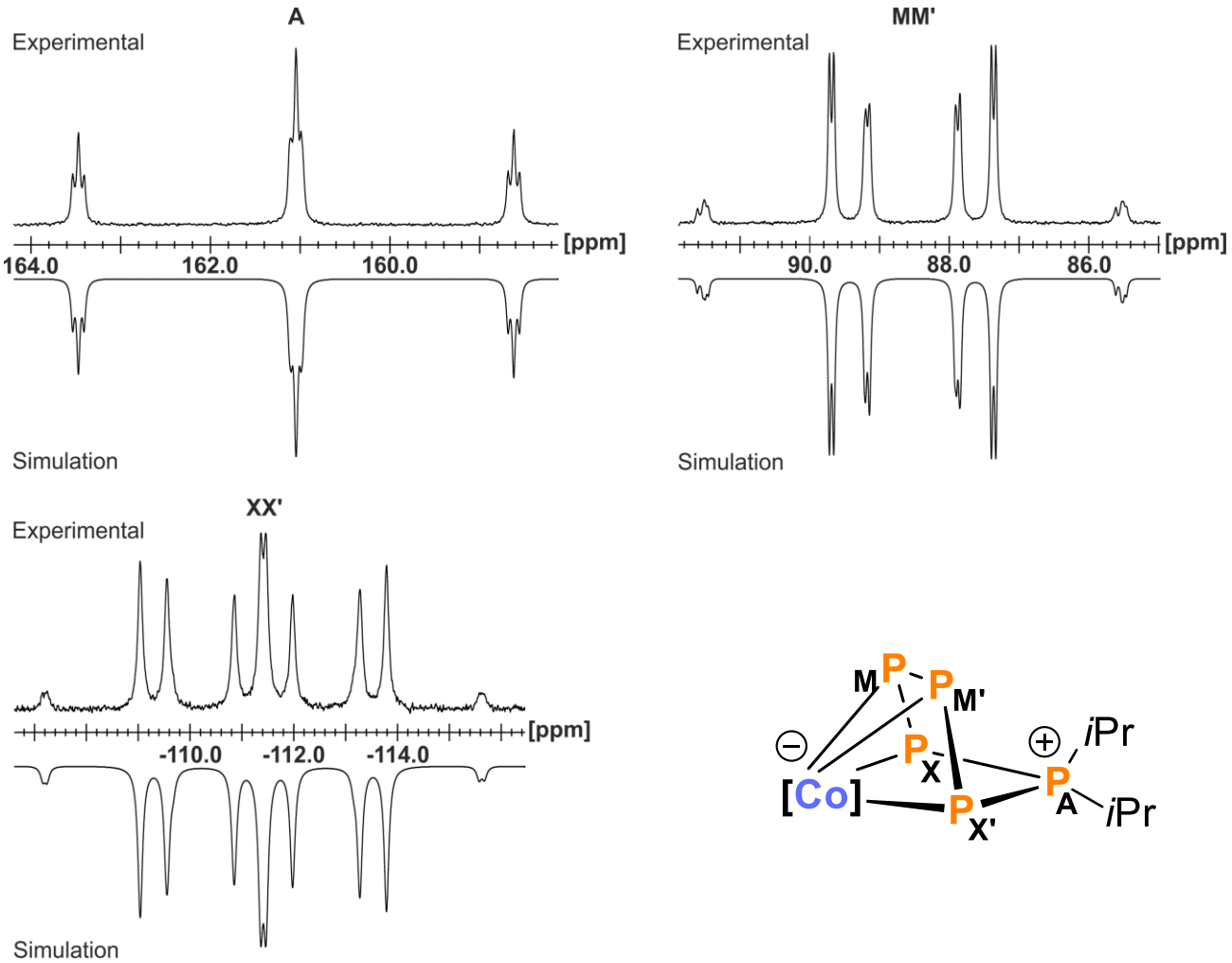

Figure S17. Section of the $^{31}P\{^{1}H\}$ NMR (400.13 MHz, 300 K, C_6D_6) of [(^{Mes}BIAN)Co(cyclo-P_5iPr$_2$)] (**3a**) and schematic representation of the CoP_5iPr$_2$ core; experimental (upwards) and simulation (downwards); [Co] = (^{Mes}BIAN)Co.

Table S3. Coupling constants from the iterative fit of the AMM'XX' spin system of [(^{Mes}BIAN)Co(cyclo-P_5iPr$_2$)] (**3a**).

$^1J_{AX} = {}^1J_{AX'}$	−392.9 Hz	$^2J_{MX'} = {}^2J_{M'X}$	39.9 Hz
$^1J_{MM'}$	−380.6 Hz	$^2J_{AM} = {}^2J_{AM'}$	10.4 Hz
$^1J_{MX} = {}^1J_{M'X'}$	−414.2 Hz	$^2J_{XX'}$	9.2 Hz

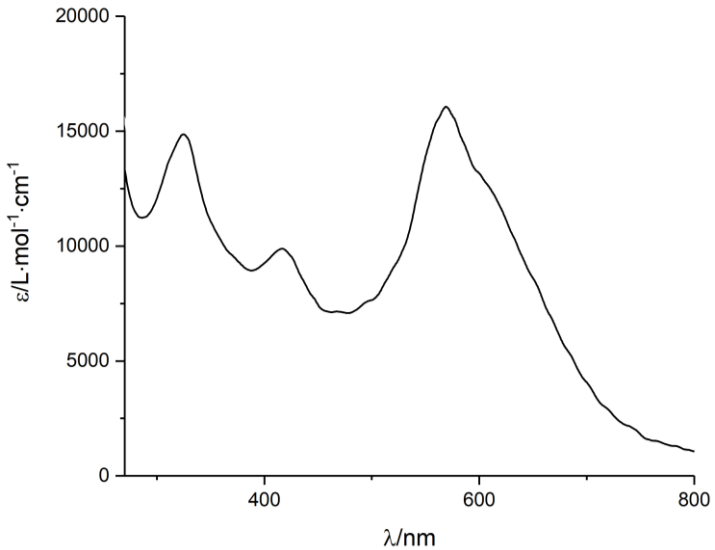

Figure S18. UV/vis spectrum of [(^{Mes}BIAN)Co(cyclo-P_5iPr$_2$)] (**3a**) recorded in THF.

Synthesis of [(^Mes^BIAN)Co(cyclo-P$_5$*t*Bu$_2$)] (3b)

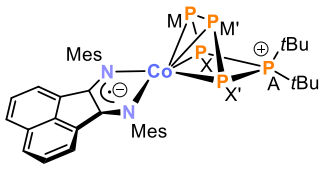

A solution of *t*Bu$_2$PCl in THF (0.5 mL, c = 0.24 mol·L^{-1}, 1.0 equiv.) was added to a dark violet THF solution (15 mL) of [K(dme)$_2${(^Mes^BIAN)Co(μ-η^4:η^2-P$_4$)Ga(nacnac)}] (**2**) (150 mg, 0.12 mmol, 1.0 equiv.). The reaction mixture was stirred while heating to 60 °C for 2 days accompanied by a color change of the solution to cyan. Separation from by-product [Ga(nacnac)] was achieved by column chromatography (stationary phase: neutral aluminum oxide, activity grade: Super I, 20 x 2 cm, eluent: *n*-hexane/toluene gradient, 100/0 to 0/100). [Ga(nacnac)] hydrolyses on aluminum oxide to nacnacH, which elutes first as colorless band (R$_f$ (*n*-hexane/toluene, 7/1 = 0.6). The following blue band (R$_f$ (*n*-hexane/toluene, 7/1 = 0.2) was collected, and the solvent was removed completely under vacuum. The remaing blue solid was extracted with *n*-hexane. Pure crystalline product **3b** precipitated from a concentrated solution of *n*-hexane at room temperature in the course of three days.

Yield: 29.7 mg (32%); m.p. 254 °C (decomposition to violet oil); UV/vis: (THF, λ$_{max}$ / nm, ε$_{max}$ / L·mol^{-1}·cm^{-1}): 295sh (9000), 332 (13000), 393 (7400), 440 (6558), 572 (9100) 629 (9769); ^{1}H NMR (400.13 MHz, 300 K, C$_6$D$_6$): δ / ppm = 7.30 (d, $^3J_{HH}$ =8.1 Hz, 2H, CH$_{(BIAN)}$), 6.96 (s, 4H. *m*-CH$_{(Mes)}$), 6.75 (dd, $^3J_{HH}$ =7.0 Hz, $^3J_{HH}$ =8.1 Hz, 2H, CH$_{(BIAN)}$), 6.45 (d, $^3J_{HH}$ =7.0 Hz, 2H, CH$_{(BIAN)}$), 2.48 (s, 12H, *o*-CH$_{3(Mes)}$), 2.26 (s, 6H, *p*-CH$_{3(Mes)}$), 1.65 (d, $^3J_{HP}$ = 12.8 Hz, 9H, C(CH$_3$)$_3$), 0.41 (d, $^3J_{HP}$ = 13.9 Hz, 9H, C(CH$_3$)$_3$); ^{13}C{^{1}H} NMR (100.61 MHz, 300 K, THF-*d*$_8$): δ / ppm = 154.2 (C$_{(BIAN)}$), 148.8 (C$_{(Mes)}$), 139.5 (C$_{(BIAN)}$), 135.0 (C$_{(Mes)}$), 132.9 (C$_{(BIAN)}$), 131.5 (C$_{(BIAN)}$), 130.9 (C$_{(Mes)}$), 129.3 (*C*H$_{(Mes)}$), 128.8 (*C*H$_{(BIAN)}$), 125.1 (*C*H$_{(BIAN)}$), 118.9 (*C*H$_{(BIAN)}$) 43.7 (*C*(CH$_3$)), 43.6 (*C*(CH)$_3$)), 33.3 (C(*C*H)$_3$)), 28.3 (C(*C*H)$_3$)), 21.2 (*p*-*C*H$_{3(Mes)}$), 19.4 (*o*-*C*H$_{3(Mes)}$); ^{31}P{^{1}H} NMR (161.98 MHz, 300 K, C$_6$D$_6$): (AMM'XX') spin system δ / ppm = 172.9 (m, 1P$_A$), 74.0 (m, 2P$_{MM'}$), −173.9 (m, P$_{XX'}$); elemental analysis calcd. for C$_{38}$H$_{46}$CoN$_2$P$_5$ (Mw = 744.60 g·mol^{-1}): C 61.30, H 6.23, N 3.76; found C 61.66, H 6.38; N 3.45.

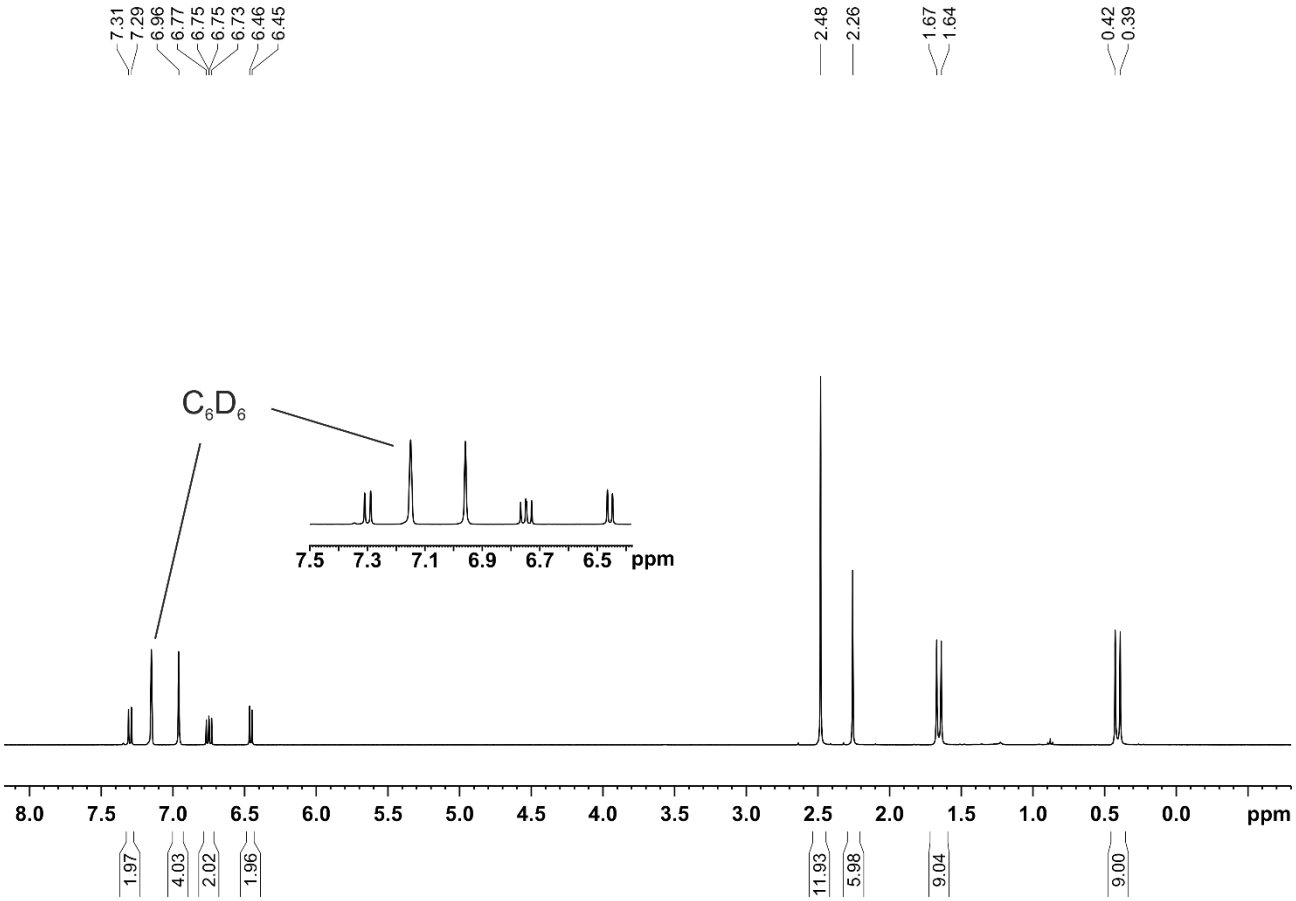

Figure S19. ^{1}H NMR spectrum (400.13 MHz, 300 K, C$_6$D$_6$) of [(^Mes^BIAN)Co(cyclo-P$_5$*t*Bu$_2$)] (**3b**).

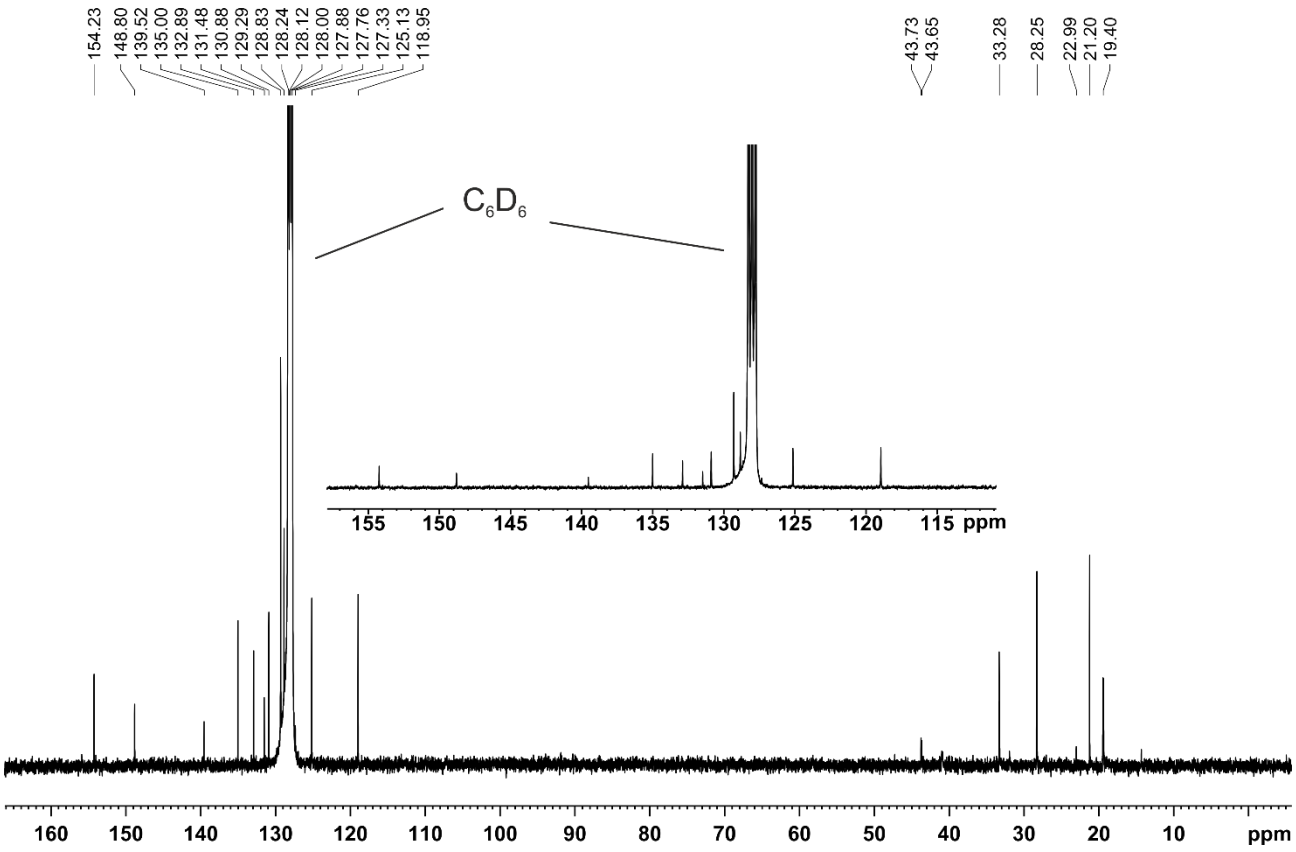

Figure S20. $^{13}C\{^{1}H\}$ NMR spectrum (100.61 MHz, 300 K, C_6D_6) of [(^{Mes}BIAN)Co(cyclo-P_5tBu$_2$)] (**3b**).

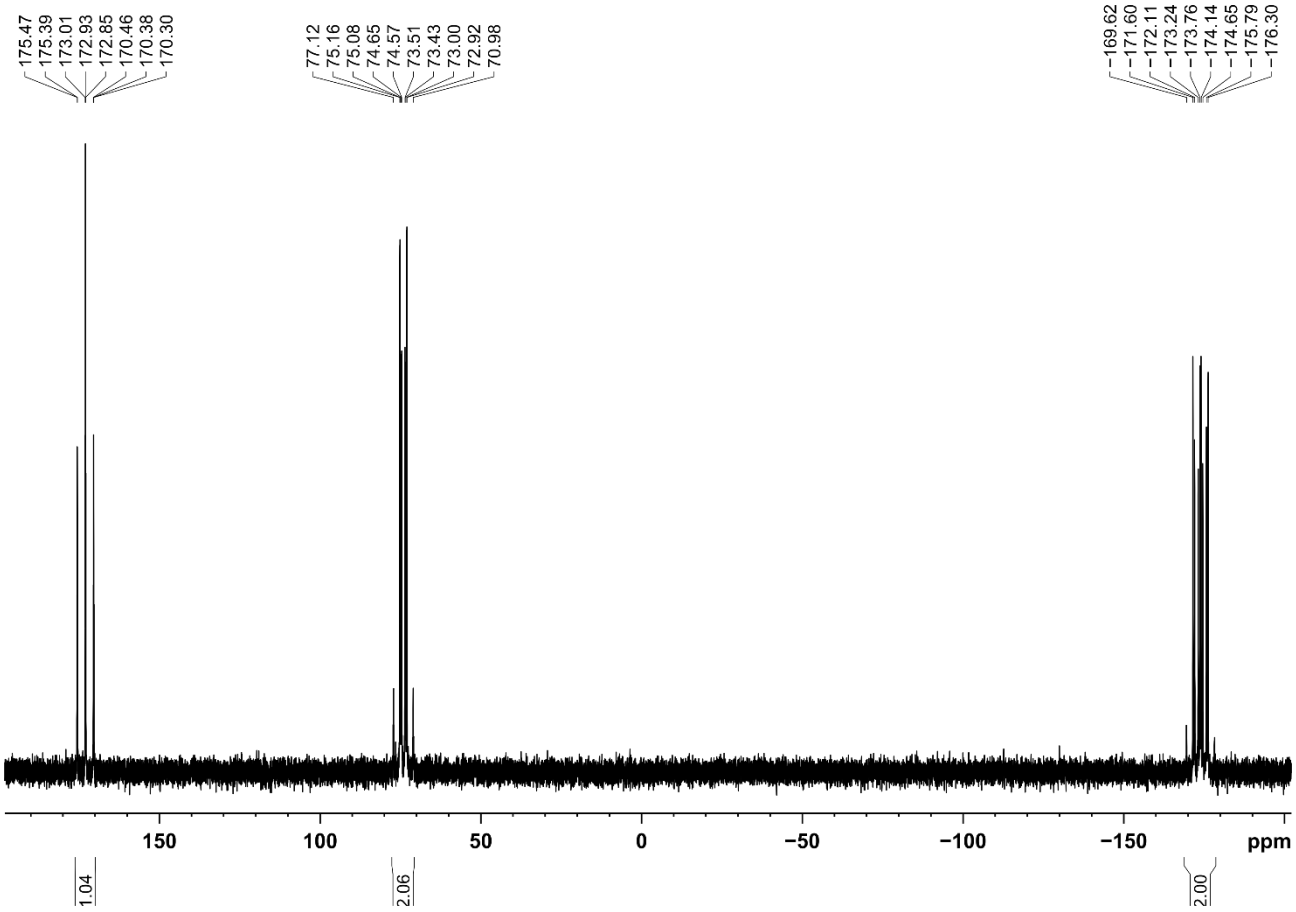

Figure S21. $^{31}P\{^{1}H\}$ NMR spectrum (161.98 MHz, 300 K, C_6D_6) of [(^{Mes}BIAN)Co(cyclo-P_5tBu$_2$)] (**3b**).

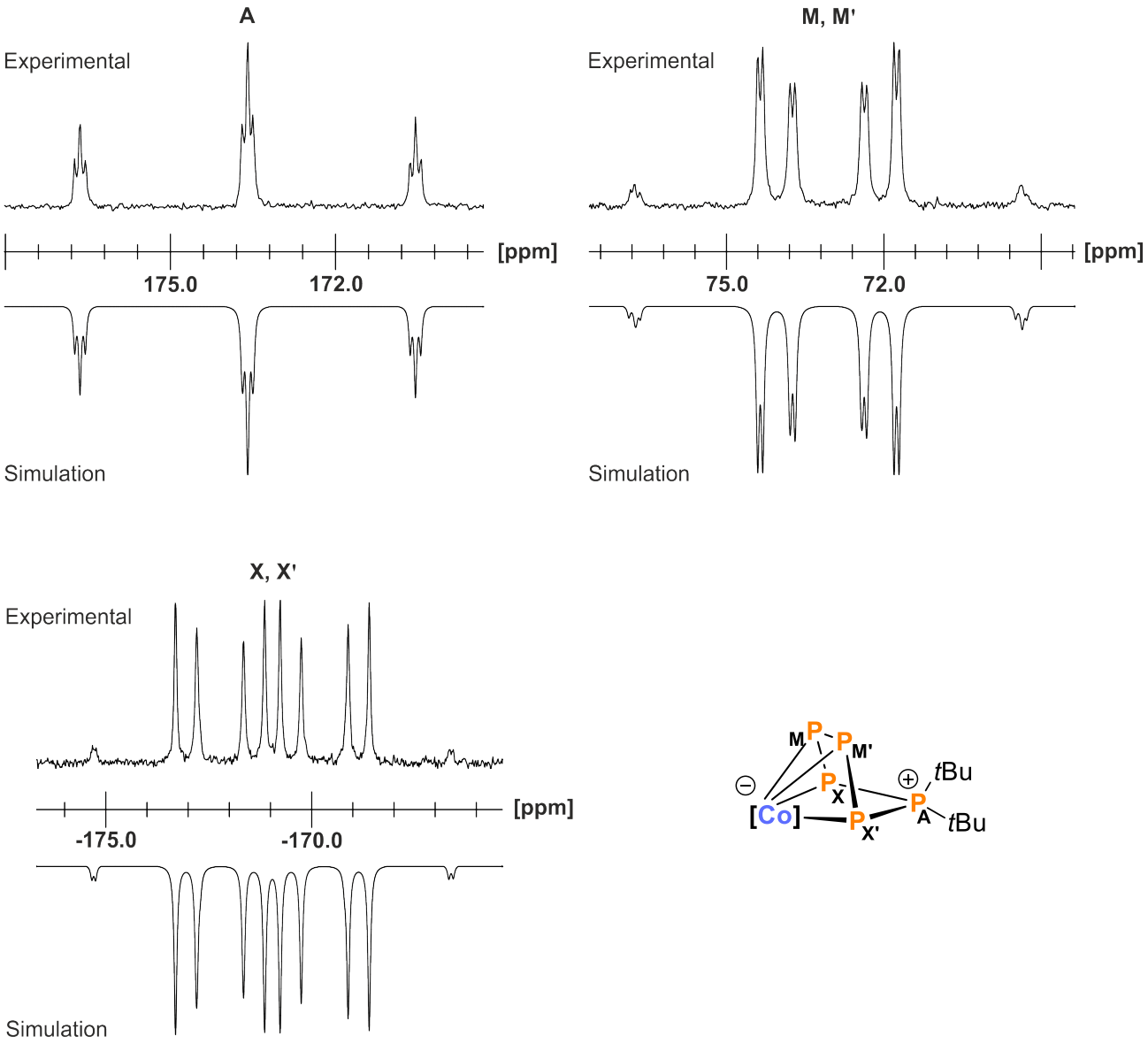

Figure S22. Section of the $^{31}P\{^{1}H\}$ NMR (400.13 MHz, 300 K, C_6D_6) of [(^{Mes}BIAN)Co(cyclo-P_5tBu$_2$)] (**3b**) and schematic representation of the CoP_5tBu$_2$ core; experimental (upwards) and simulation (downwards); [Co] = (^{Mes}BIAN)Co.

Table S4. Coupling constants from the iterative fit of the AMM'XX' spin system of [(^{Mes}BIAN)Co(cyclo-P_5tBu$_2$)] (**3b**).

$^1J_{AX} = {}^1J_{AX'}$	−411.4 Hz	$^2J_{MX'} = {}^2J_{M'X}$	38.8 Hz
$^1J_{MM'}$	−405.3 Hz	$^2J_{AM} = {}^2J_{AM'}$	13.1 Hz
$^1J_{MX} = {}^1J_{M'X'}$	−389.4 Hz	$^2J_{XX'}$	9.6 Hz

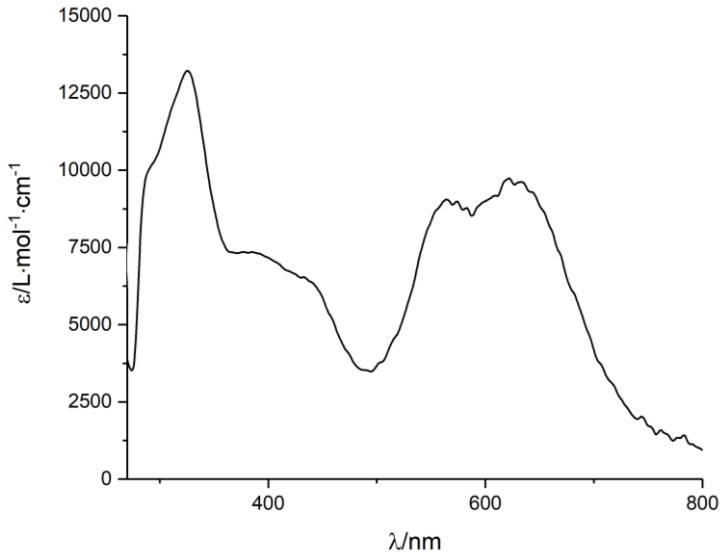

Figure S23. UV/vis spectrum of [(^{Mes}BIAN)Co(cyclo-P$_5$*t*Bu$_2$)] (**3b**) recorded in THF.

Synthesis of [(^{Mes}BIAN)Co(cyclo-P$_5$Cy$_2$)] (3c)

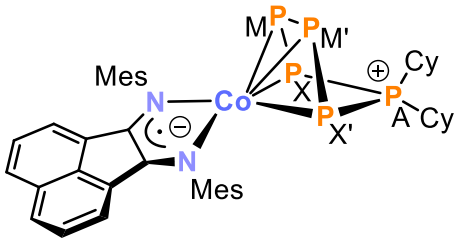

A solution of Cy$_2$PCl in THF (2.1 mL, c = 0.12 mol·L^{-1}, 1.0 equiv.) was added to a dark violet THF solution (10 mL) of [K(dme)$_2${(^{Mes}BIAN)Co(μ-η^4:η^2-P$_4$)Ga(nacnac)}] (**2**) (335.5 mg, 0.25 mmol, 1.0 equiv.) and stirred at 60 °C for 2 days. A color change of the reaction mixture to cyan was observed. The by-product [Ga(nacnac)] was separated by column chromatography (stationary phase: neutral aluminum oxide activity grade: Super I, 10 x 2 cm, eluent: *n*-hexane/toluene gradient, 100/0 to 0/100). [Ga(nacnac)] hydrolyses on aluminum oxide to nacnacH, which elutes first as colorless band (R_f (*n*-hexane/toluene, 7/1 = 0.6). The following blue band (R_f (*n*-hexane/toluene, 7/1 = 0.2) was collected, the obtained solution concentrated in *vacuo* and crystallization by *n*-hexane diffusion gave X-ray quality crystals of **3c** after three days storage at room temperature.

Yield: 54.5 mg (26%); m.p. 252 °C (decomposition to violet oil); UV/vis: (THF, λ_{max} / nm, ε_{max} / L·mol^{-1}·cm^{-1}): 332 (14000), 424 (9000), 574 (14000), 580 (14500); ^{1}H NMR (400.13 MHz, 300 K, C$_6$D$_6$): δ / ppm = 7.32 (d, $^3J_{HH}$ =8.2 Hz, 2H, CH$_{(BIAN)}$), 6.99 (s, 4H. *m*-CH$_{(Mes)}$), 6.73 (*pseudo*-t, $^3J_{HH}$ =7.4 Hz, $^3J_{HH}$ =7.8 Hz, 2H, CH$_{(BIAN)}$), 6.49 (d, $^3J_{HH}$ =6.8 Hz, 2H, CH$_{(BIAN)}$), 2.47 (s, 12H, *o*-CH$_{3(Mes)}$), 2.33 (s,6H, *p*-CH$_{3(Mes)}$), 1.94 (m, 2H, CH$_{2(cy)}$), 1.55 (m, 3H, CH$_{2(cy)}$ and CH$_{(cy)}$), 1.34 – 1.0 (m, 10H, CH$_{2(cy)}$), 0.93 – 0.64 (m, 4H, CH$_{2(cy)}$), 0.65 – 0.49 (m, 3H, CH$_{2(cy)}$ and CH$_{(cy)}$); ^{13}C{^{1}H} NMR (100.61 MHz, 300 K, THF-*d*$_8$): δ / ppm = 154.5 (C$_{(BIAN)}$), 153.6 (C$_{(Mes)}$), 139.3 (C$_{(BIAN)}$), 134.8 (C$_{(Mes)}$), 133.0 (C$_{(BIAN)}$), 131.8 (C$_{(BIAN)}$), 129.7 (C$_{(Mes)}$), 129.5 (*C*H$_{(Mes)}$), 129.0 (*C*H$_{(BIAN)}$), 125.0 (*C*H$_{(BIAN)}$), 118.7 (*C*H$_{(BIAN)}$), 40.0 (C$_{Cy}$), 39.8 (C$_{Cy}$), 32.3 (br, C$_{Cy}$), 29.3 (br, C$_{Cy}$), 26.8 (C$_{Cy}$), 26.7 (C$_{Cy}$), 26.4 (C$_{Cy}$), 26.3 (C$_{Cy}$), 25.9 (C$_{Cy}$), 25.4 (C$_{Cy}$), 21.2 (*p*-*C*H$_{3(Mes)}$), 19.0 (*o*-*C*H$_{3(Mes)}$); ^{31}P{^{1}H} NMR (161.98 MHz, 300 K, C$_6$D$_6$): (AMM'XX') spin system δ / ppm = 154.0 (m, 1P$_A$), 87.9 (m, 2P$_{MM'}$), −113.2 (m, P$_{XX'}$); elemental analysis calcd. for C$_{42}$H$_{50}$CoN$_2$P$_5$ · (C$_7$H$_8$)$_{0.5}$ · (C$_6$H$_{14}$)$_{0.1}$ (Mw = 851.35g·mol^{-1}): C 65.04, H 6.56, N 3.29; found C 65.48, H 6.44; N 3.22. According to ^{1}H NMR spectroscopy the compound contains 0.5 molecules toluene and approximately 0.1 molecules *n*-hexane per formula unit after drying under vacuum (10^{-3} mbar).

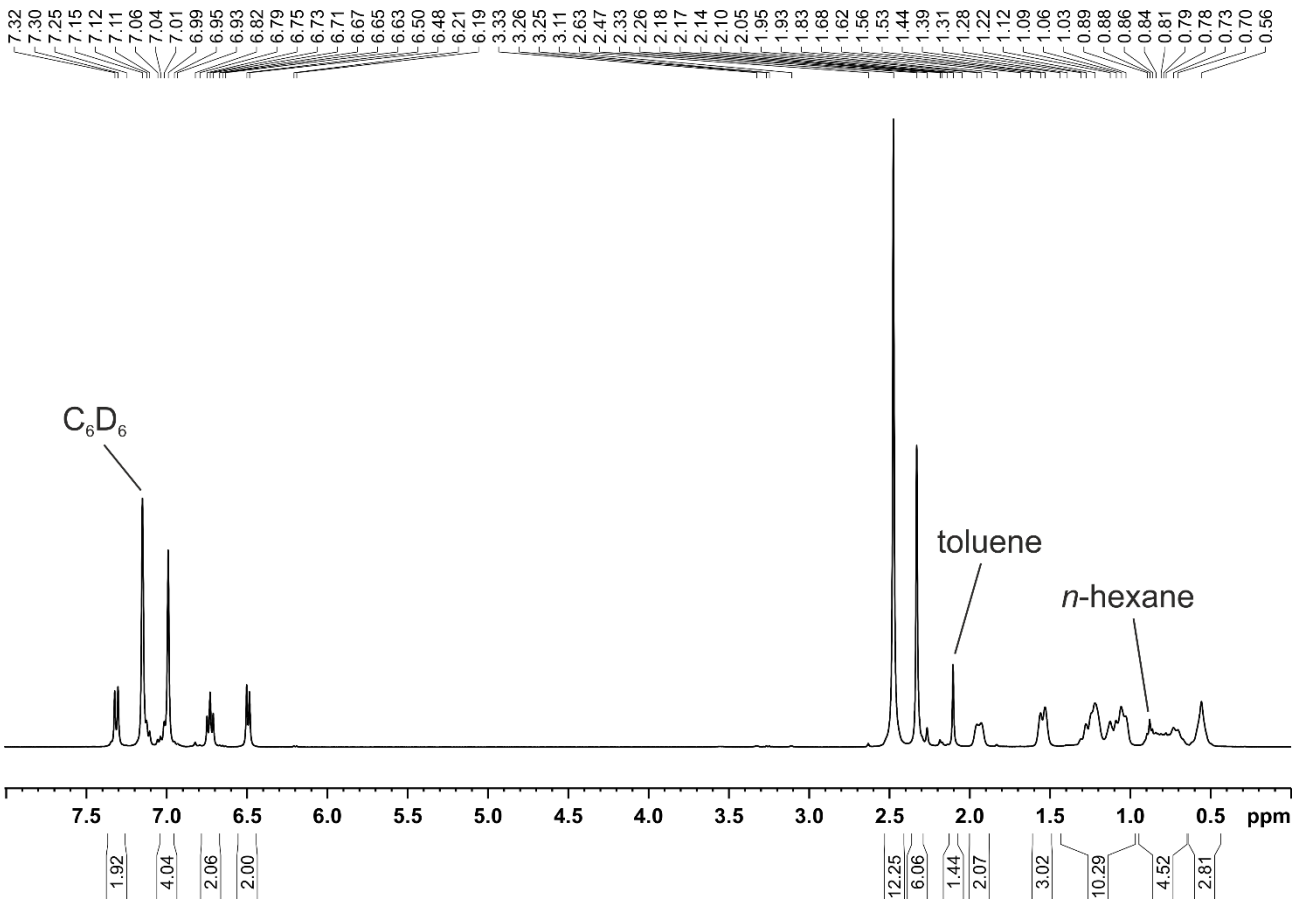

Figure S24. ^{1}H NMR spectrum (400.13 MHz, 300 K, C_6D_6) of [(^{Mes}BIAN)Co(cyclo-P_5Cy_2)] (**3c**).

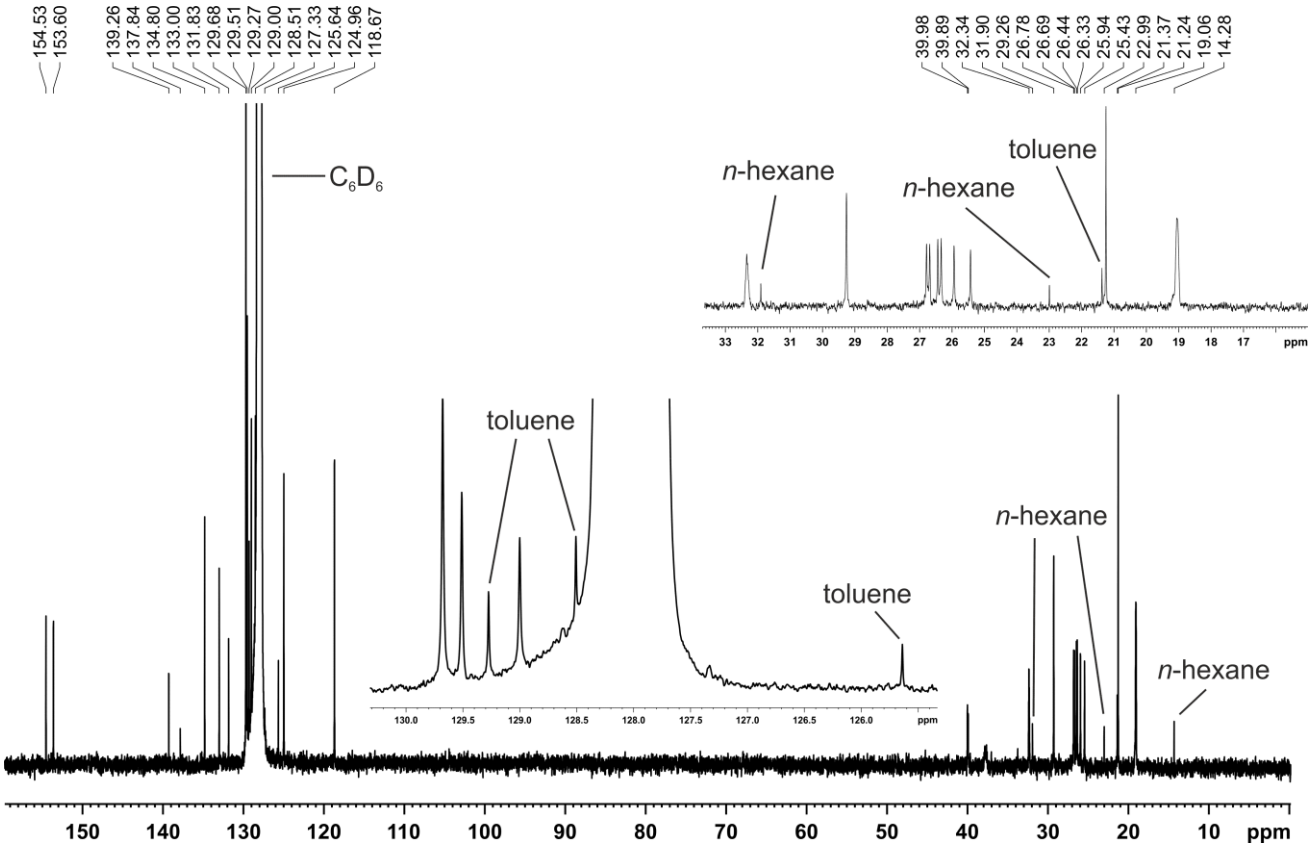

Figure S25. ^{13}C{^{1}H} NMR spectrum (100.61 MHz, 300 K, C_6D_6) of [(^{Mes}BIAN)Co(cyclo-P_5Cy_2)] (**3c**).

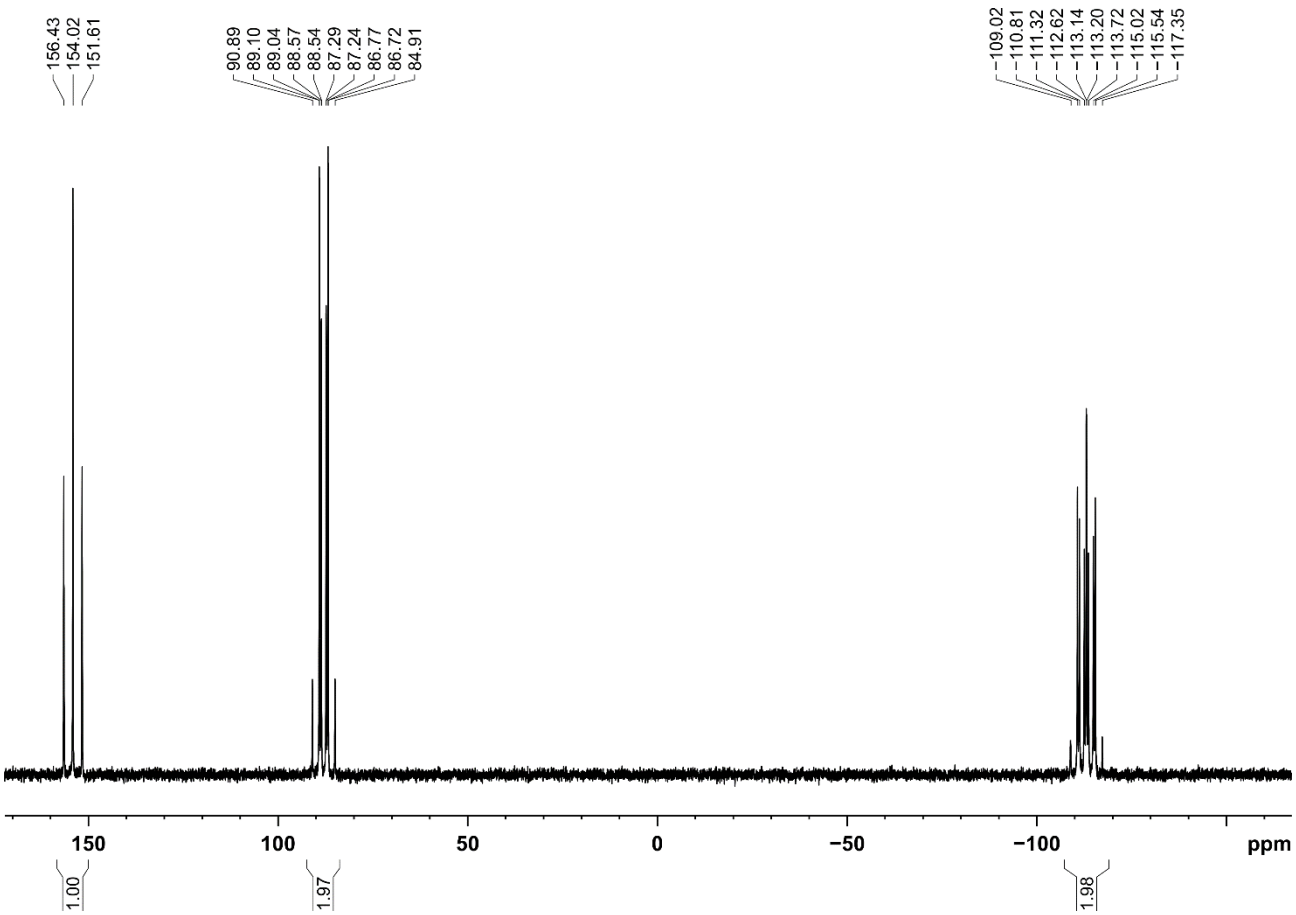

Figure S26. $^{31}P\{^{1}H\}$ NMR spectrum (161.98 MHz, 300 K, C_6D_6) of [(^{Mes}BIAN)Co(cyclo-P_5Cy_2)] (**3c**).

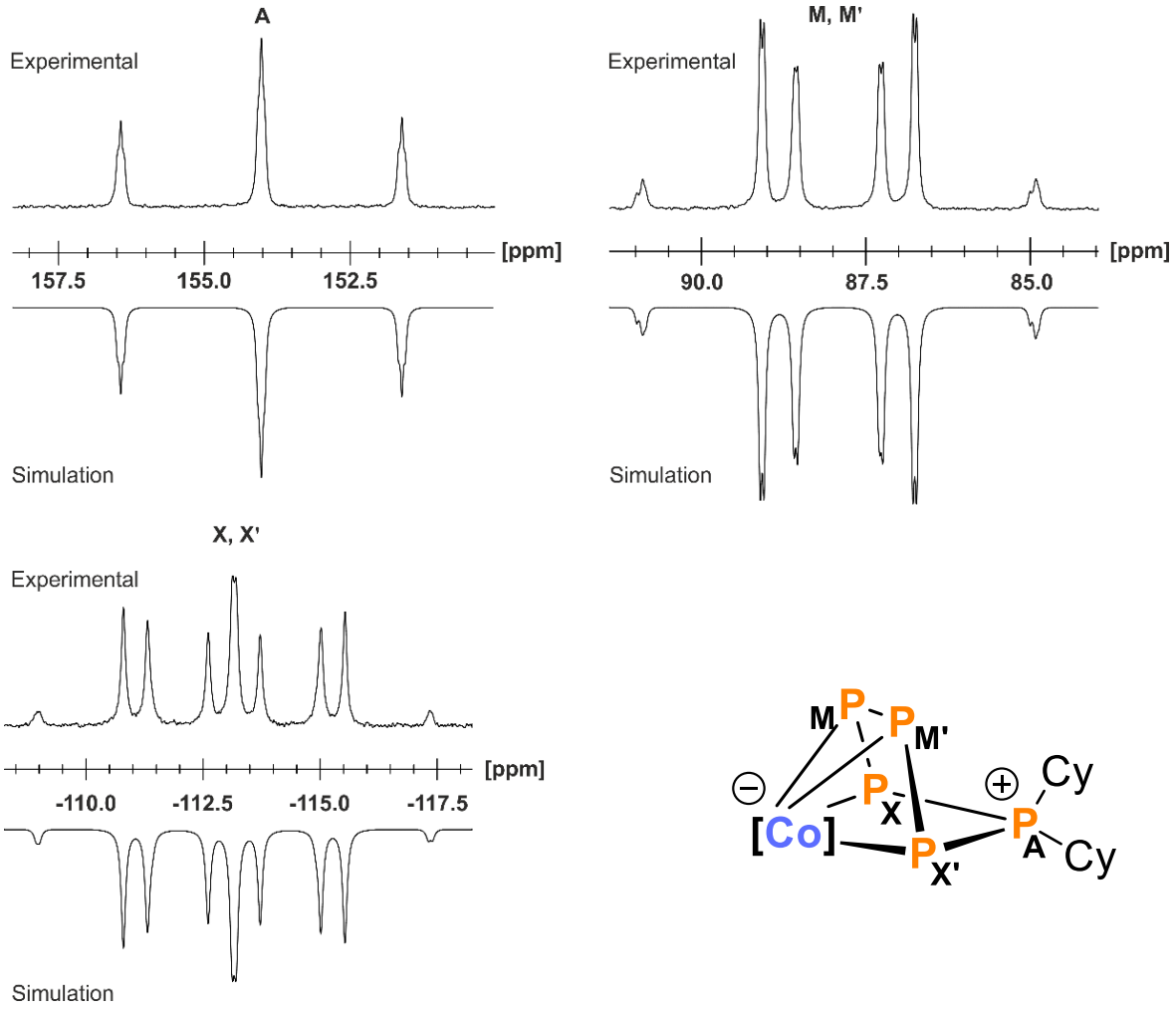

Figure S27. Section of the $^{31}P\{^{1}H\}$ NMR (400.13 MHz, 300 K, C_6D_6) of [(^{Mes}BIAN)Co(cyclo-P_5Cy_2)] (**3c**) and schematic representation of the CoP_5Cy_2 core; experimental (upwards) and simulation (downwards); [Co] = (^{Mes}BIAN)Co.

Table S5. Coupling constants from the iterative fit of the AMM'XX' spin system of [(^{Mes}BIAN)Co(cyclo-P_5Cy_2)] (**3c**).

$^1J_{AX} = {}^1J_{AX'}$	−390.1 Hz	$^2J_{MX'} = {}^2J_{M'X}$	37.5 Hz
$^1J_{MM'}$	−379.0 Hz	$^2J_{AM} = {}^2J_{AM'}$	9.5 Hz
$^1J_{MX} = {}^1J_{M'X'}$	−413.5 Hz	$^2J_{XX'}$	8.0 Hz

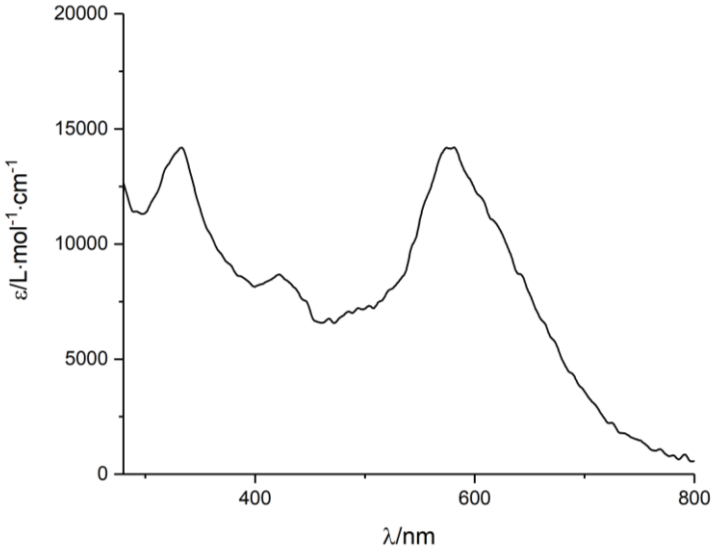

Figure S28. UV/vis spectrum of [(MesBIAN)Co(cyclo-P_5Cy_2)] (**3c**) recorded in THF.

Intermediate [(MesBIAN)Co(μ-η⁴:η²-P₅*i*Pr₂)Ga(nacnac)}] (4)

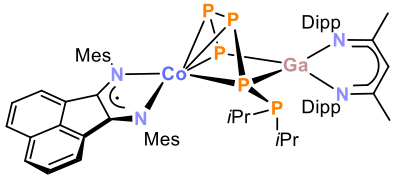

A solution of *i*Pr₂PCl in THF (0.38 mL, c = 0.18 mol·L^{-1}, 1.0 equiv.) was added to a dark violet THF solution (10 mL) of [K(dme)₂{(MesBIAN)Co(μ-η⁴:η²-P₄)Ga(nacnac)}] (**2**) (85 mg, 0.07 mmol, 1.0 equiv.) and stirred for 30 minutes. Volatiles were removed in *vacuo* and the remaining violet residue was extracted with 20 mL *n*-hexane. Violet crystals of **4** suitable for single X-ray diffraction formed during storage at −30 °C in the course of two days.

The instability of compound **4** in solution prevented its further characterization. **4** readily transform to compound **3a** in solution (*vide infra*).

Synthesis of [(MesBIAN)Co(μ-η⁴:η¹-P₅*t*Bu)GaCl(nacnac)] (5)

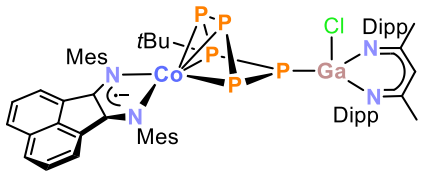

A solution of *t*BuPCl₂ in THF (2.0 mL, c = 0.12 mol·L^{-1}, 1.0 equiv.) was added to a dark violet THF solution (15 mL) of [K(dme)₂{(MesBIAN)Co(μ-η⁴:η²-P₄)Ga(nacnac)}] (**2**) (300 mg, 0.24 mmol, 1.0 equiv.). The mixture turned greyish-blue and was stirred for two days at room temperature. Subsequently, all volatiles were removed in *vacuo*. The remaining dark solid was redissolved in toluene (10 mL, greyish-blue solution) and filtered through a P4 frit. The ^{1}H NMR spectrum (400.13 MHz, 300 K, THF-d_8) of the raw product shows the signals of the main product **5** and signals assigned to an unidentified paramagnetic impurity [δ / ppm = 48.6 (br), 41.4, 18.9, 6.5 (br) 1.3, −6.1 (br), −8.2, −16.6 (br)]. The paramagnetic impurity was removed by recrystallizing the raw product six times from concentrated toluene solution at −30 °C. According to the ^{1}H NMR spectrum, the isolated compound subsequently only contained traces of the paramagnetic impurity. Based in the ^{1}H NMR data, 0.74 toluene solvate molecules per formula unit were present after evacuating the solid for 5 h at room temperature. Crystals suitable for single X-ray diffraction were obtained by slow evaporation of fluorobenzene solution over the course of three weeks.

Yield: 18.4 mg (6%); m.p. 255 °C (decomposition to black oil); UV/vis: (THF, λ_{max} / nm, ε_{max} / L·mol^{-1}·cm^{-1}): 348(30000), 421 (12000), 612 (15500); ^{1}H NMR (400.13 MHz, 300 K, THF-d_8): δ / ppm = 7.63 (d, *J* = 8.0, 2H, CH_{BIAN}), 6.98 (m, 2H, CH_{BIAN}), 7.32 – 7.03 (m, 6H, CH_{Dipp}), 7.01 – 6.96 (m, 2H CH_{BIAN}), 6.96 – 6.90 (m,4H, CH_{Mes}), 6.19 (d, $^3J_{HH}$ = 6.2 Hz, 2H, CH_{BIAN}), 5.15 (s, 1H, CH_{nacnac}), 3.24 – 3.05 (m, 3H, C*H*$(CH_3)_2$), 2.77 (sept, $^3J_{HH}$ = 6.8 Hz, 2H, C*H*$(CH_3)_2$), 2.41 (s, 6H, $CH_{3(Mes)}$), 2.21 (s, 6H, $CH_{3(Mes)}$), 1.92 (s, 6H, $CH_{3(Mes)}$) 1.77 (s, 3H, $CH_{3(nacnac)}$), 1.73 (s, 3H, $CH_{3(nacnac)}$), 1.55 (d, $^3J_{HH}$ = 6.7 Hz, 3H, CH(C*H*$_3)_2$), 1.45 (d, $^3J_{HH}$ = 6.6 Hz, 3H, CH(C*H*$_3)_2$), 1.36 (d, $^3J_{HH}$ = 6.8 Hz, 3H, CH(C*H*$_3)_2$), 1.18 – 1.12 (m, 9H, CH(C*H*$_3)_2$), 1.00 (m, 6H, CH(C*H*$_3)_2$), 0.89 (d, $^3J_{HP}$ = 15.5 Hz, 9H, $C(CH_3)_3$); $^{13}C\{^1H\}$ (100.61 MHz, 300 K, THF-d_8): δ / ppm = 170.3 (C_{nacnac}), 170.0 (C_{nacnac}), 156.3 (C_{BIAN}), 153.2 (C_{Mes}), 146.1 (C_{Dipp}), 145.6 (C_{Dipp}), 143.4 (C_{Dipp}), 143.3 (C_{Dipp}), 143.3 (C_{Dipp}), 141.8 (C_{BIAN}), 141.3 (C_{Dipp}), 138.4 (C_{BIAN}), 134.8 (C_{Mes}), 133.4 (C_{BIAN}), 133.3 (C_{BIAN}), 132.2 (C_{BIAN}), 129.5 (CH_{Mes}), 129.3 (CH_{Mes}), 128.9 (CH_{BIAN}), 128.8 (CH_{BIAN}), 128.7 (CH_{BIAN}), 128.3 (CH_{Dipp}), 126.2 (CH_{Dipp}), 126.0 (CH_{Dipp}), 125.9 (CH_{Dipp}), 125.4 (CH_{Dipp}), 125.3 (CH_{BIAN}),125.2 (CH_{BIAN}), 124.8 (CH_{Dipp}), 118.8

(CH_{BIAN}) 97.1 (CH_{nacnac}), 40.6 (C(CH)$_3$), 33.2 (C(CH)$_3$), 30.6 (CH(CH$_3$)$_2$), 30.2 (CH(CH$_3$)$_2$), 28.4 (CH(CH$_3$)$_2$), 28.2 (CH(CH$_3$)$_2$), 27.3 (CH(CH$_3$)$_2$) 27.6 (CH(CH$_3$)$_2$), 26.0 (CH(CH$_3$)$_2$), 25.7 (CH(CH$_3$)$_2$), 25.5 (CH(CH$_3$)$_2$), 25.3 (CH(CH$_3$)$_2$), 24.4 (CH(CH$_3$)$_2$), 23.9 (CH(CH$_3$)$_2$), 23.8 ($CH_{3(nacnac)}$), 23.7 ($CH_{3(nacnac)}$), 23.6 ($CH_{3(Mes)}$), 21.2 ($CH_{3(Mes)}$), 19.5 ($CH_{3(Mes)}$), 19.5 ($CH_{3(Mes)}$), 19.1 ($CH_{3(Mes)}$) 19.2 ($CH_{3(Mes)}$); $^{31}P\{^1H\}$ NMR (161.98 MHz, 300 K, THF-d_8): (ABEMX) spin system δ / ppm = 70.6 (m, 2P), 50.5 (m, 1P), 13.6 (m, 1P), −64.7 (m, 1P), $^{31}P\{^1H\}$ NMR (161.98 MHz, 213 K, THF-d_8): (ABEMX) spin system δ / ppm = 70.3 (m, 1P), 66.0 (m, 1P), 48.4 (m, 1P), 12.0 (m, 1P), −66.8 (m, 1P); elemental analysis calcd. for $C_{63}H_{78}ClCoGaN_4P_5 \cdot (C_4H_{10}O_2)_2 \cdot (C_7H_8)_{0.74}$ (Mw = 1278.5 g·mol^{-1}): C 64.05, H 6.62, N 4.38; found C 64.79, H 6.61, N 4.46. According to ^1H NMR spectroscopy the compound contains 0.74 molecules toluene per formula unit after drying under vacuum (10^{-3} mbar). The elemental analysis showed a higher C-value than expected for this composition indicating varying concentration of the solvate.

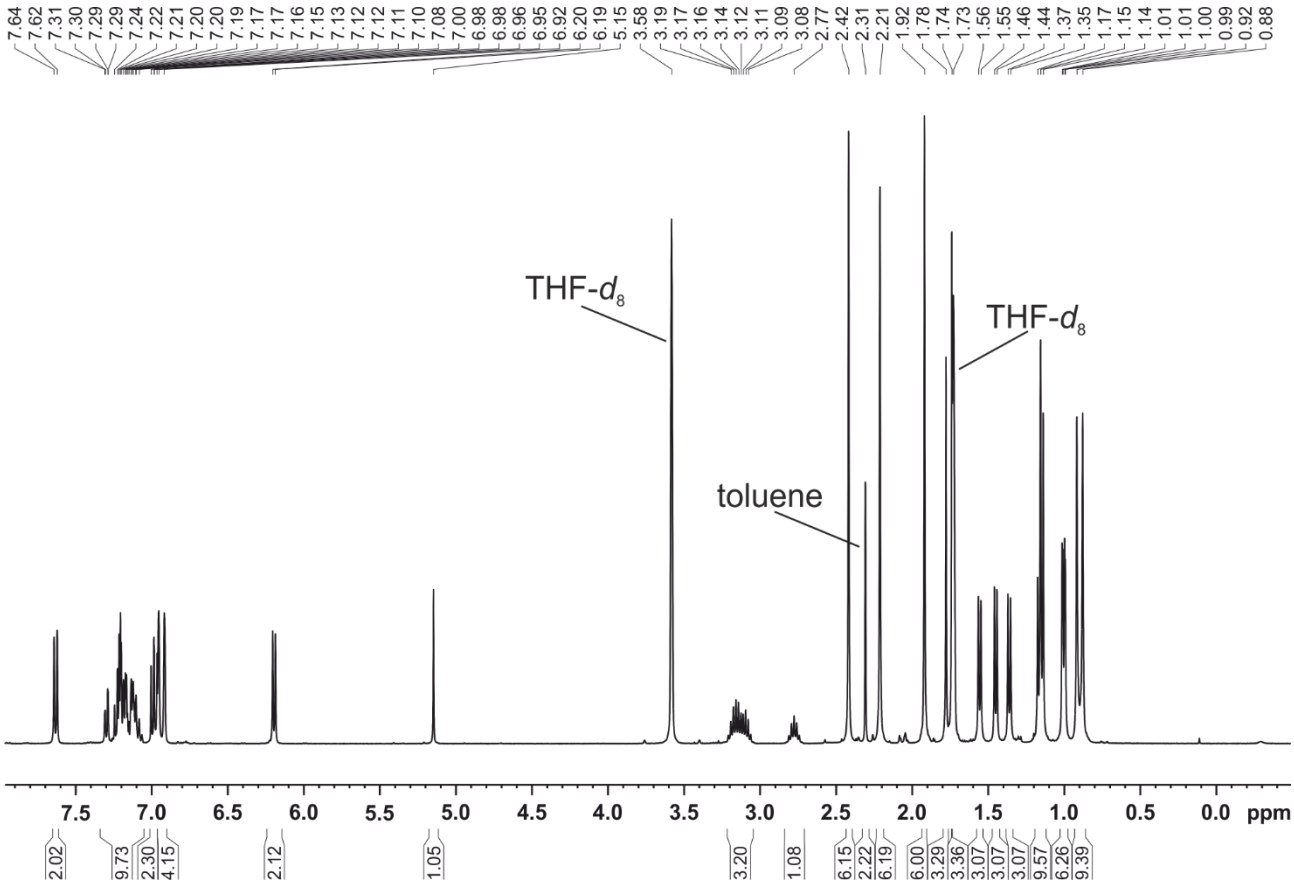

Figure S29. ^1H NMR spectrum (400.13 MHz, 300 K, THF-d_8) of [(^{Mes}BIAN)Co(μ-η^4:η^1-P$_5$$t$Bu)GaCl(nacnac)] (**5**).

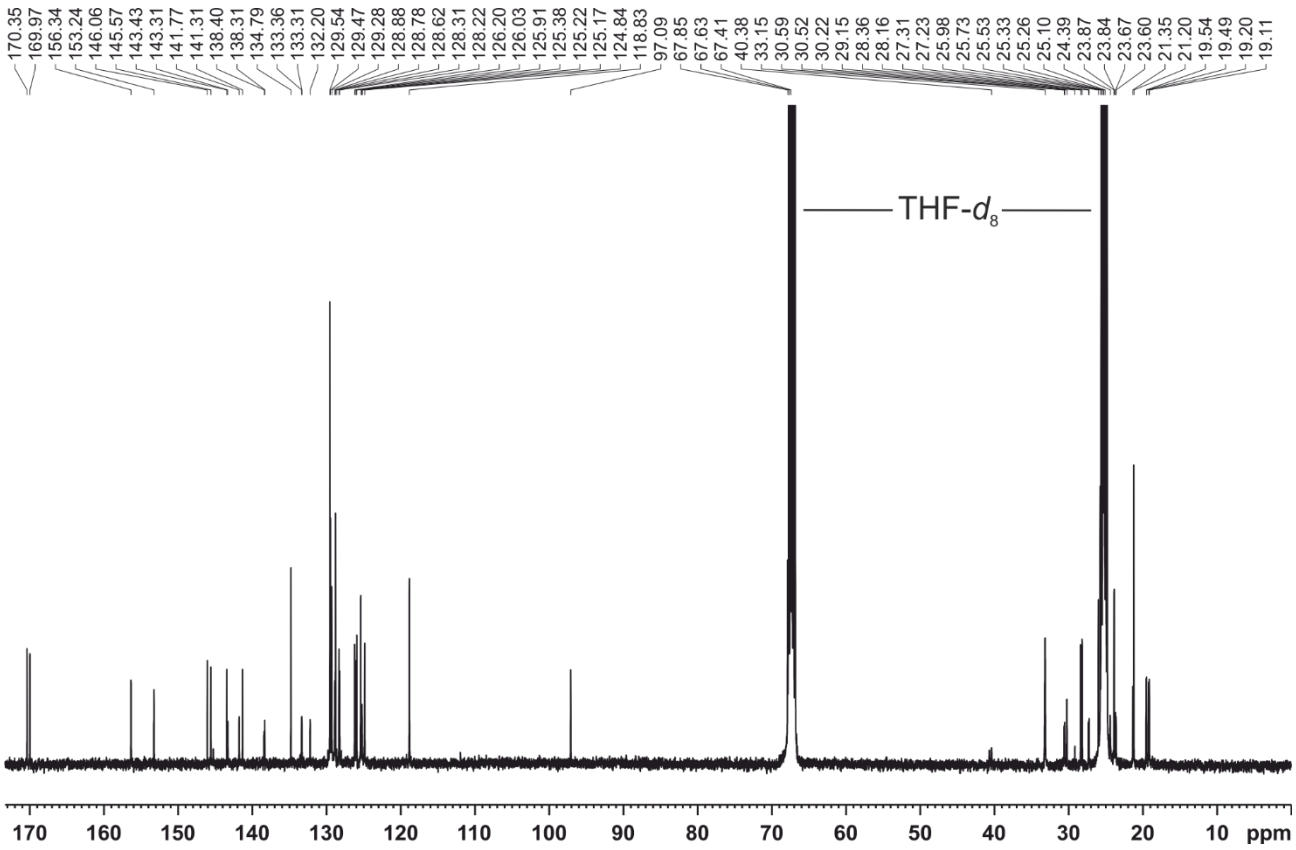

Figure S30. $^{13}C\{^1H\}$ NMR spectrum (100.61 MHz, 300 K, THF-d_8) of [(^{Mes}BIAN)Co(μ-η^4:η^1-P$_5$*t*Bu)GaCl(nacnac)] (**5**).

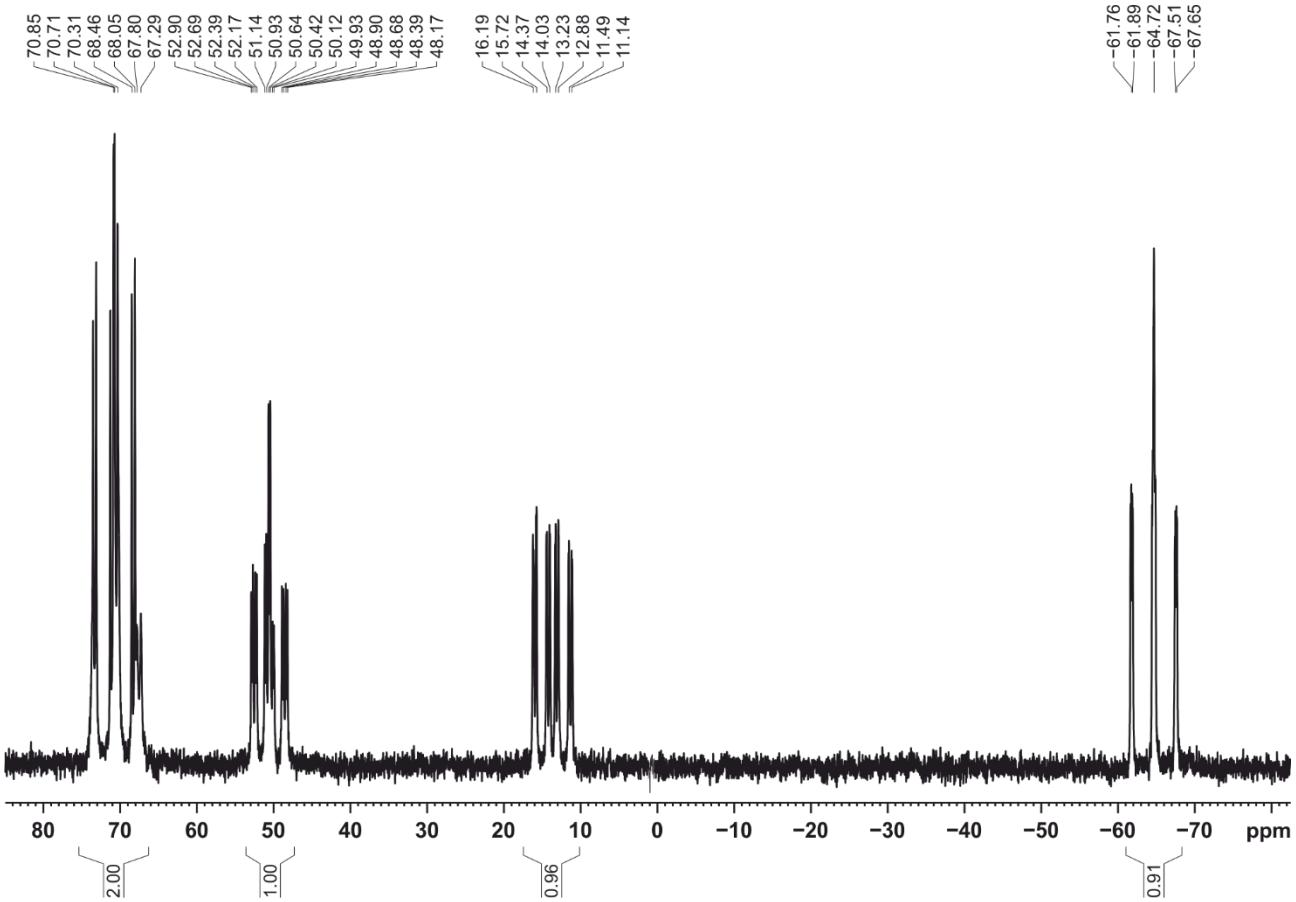

Figure S31. $^{31}P\{^1H\}$ NMR spectrum (161.98 MHz, 300 K, THF-d_8) of [(^{Mes}BIAN)Co(μ-η^4:η^1-P$_5$*t*Bu)GaCl(nacnac)] (**5**).

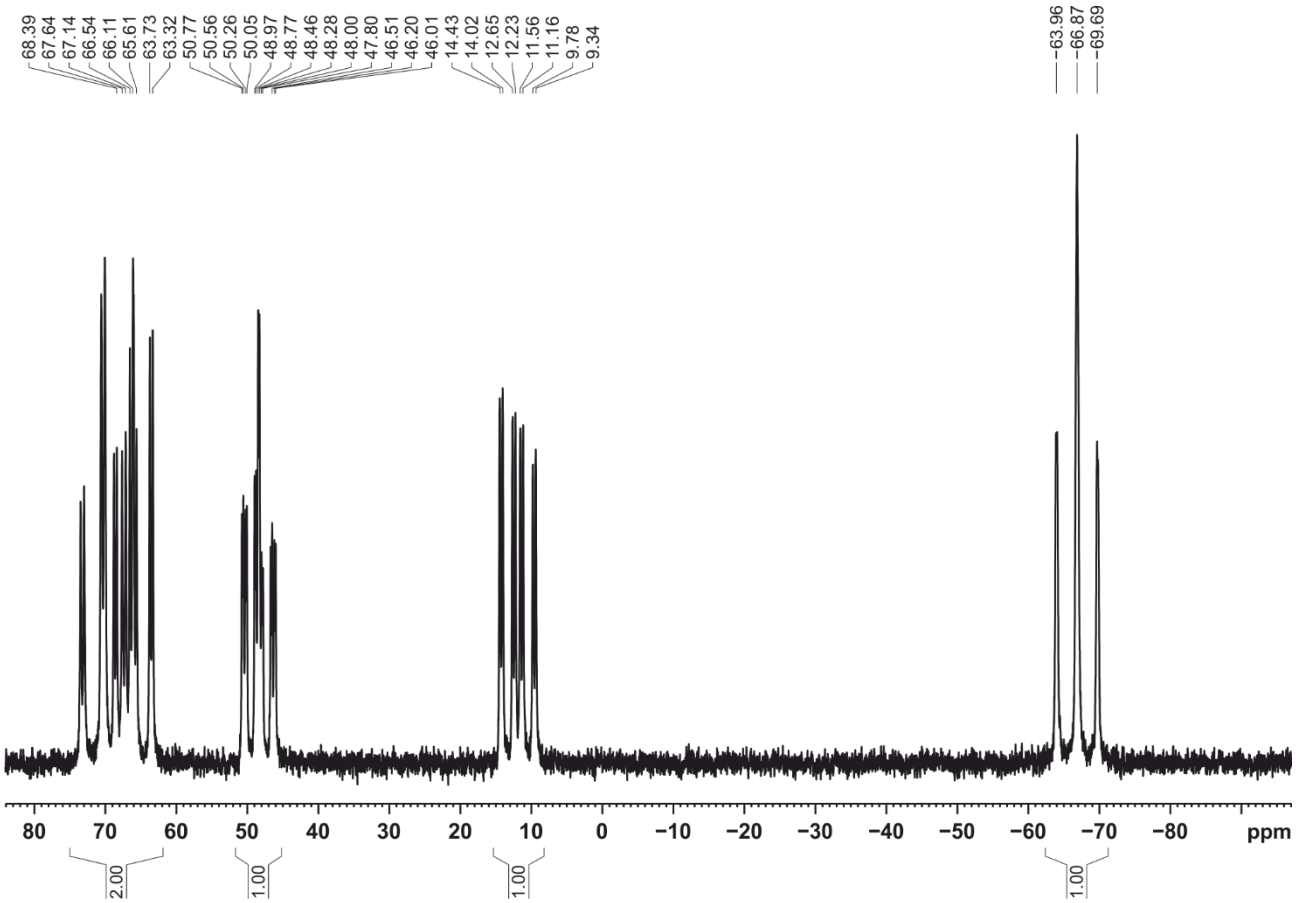

Figure S32. $^{31}P\{^{1}H\}$ NMR spectrum (161.98 MHz, 213 K, THF-d_8) of [(^{Mes}BIAN)Co(μ-η^4:η^1-P$_5$*t*Bu)GaCl(nacnac)] (**5**).

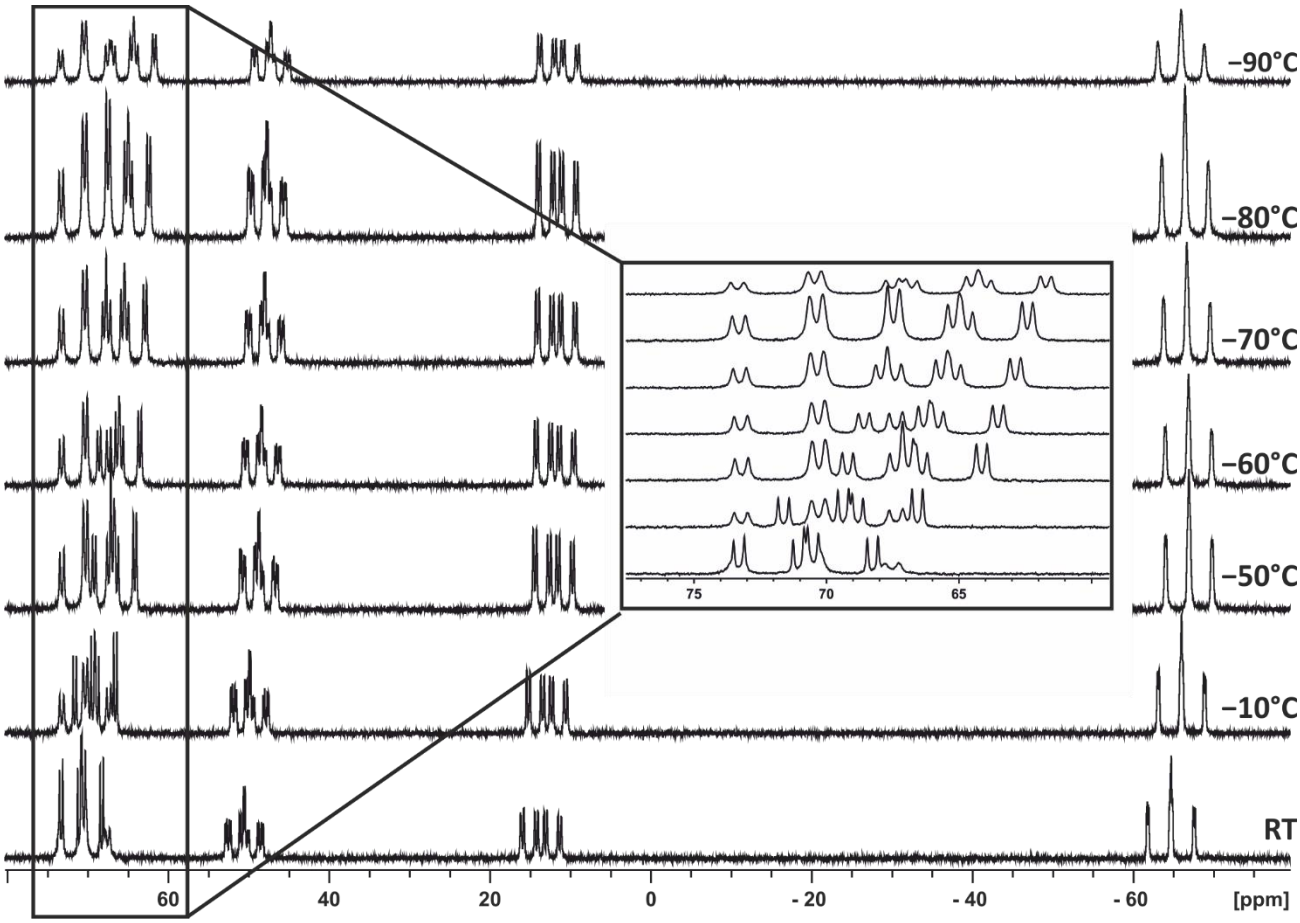

Figure S33. VT-$^{31}P\{^{1}H\}$ NMR spectrum (161.98 MHz, THF-d_8) of [(^{Mes}BIAN)Co(μ-η^4:η^1-P$_5$*t*Bu)GaCl(nacnac)] (**5**); inset section from 77.0 ppm to 60.0 ppm.

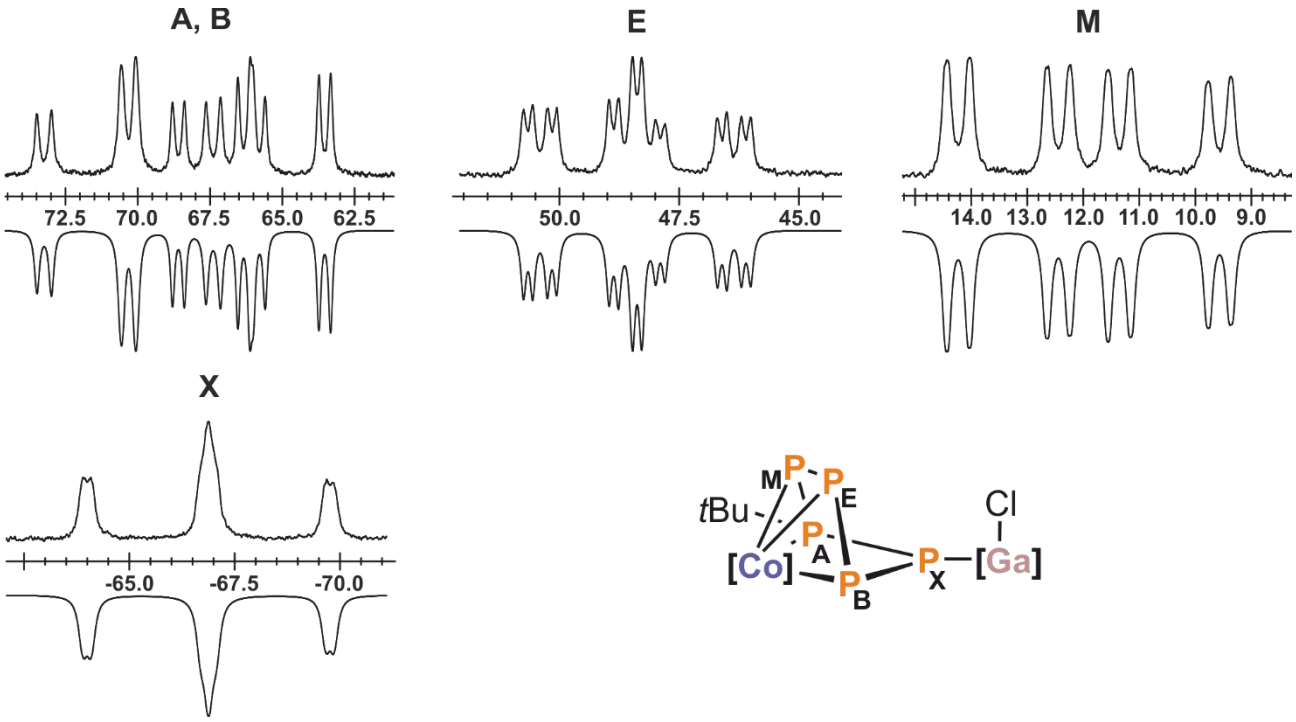

Figure S34. Section of the $^{31}P\{^{1}H\}$ NMR (400.13 MHz, 213 K, THF-d_8) of [(^{Mes}BIAN)Co(μ-η^4:η^1-P$_5$*t*Bu)GaCl(nacnac)] (**5**) and schematic representation of the CoP$_5$*t*BuGa core; experimental (upwards) and simulation (downwards); [Co] = (^{Mes}BIAN)Co, [Ga] = (nacnac)Ga.

Table S6. Coupling constants from the iterative fit of the ABEMX spin system of [(^{Mes}BIAN)Co(μ-η^4:η^1-P$_5$*t*Bu)GaCl(nacnac)] (**5**) at 213.

$^1J_{AM}$	−466.3 Hz	$^2J_{AE}$	81.8 Hz
$^1J_{AX}$	−481.4 Hz	$^2J_{ABM}$	8.2 Hz
$^1J_{BX}$	−455.1 Hz	$^2J_{BM}$	67.7 Hz
$^1J_{BE}$	−367.0 Hz	$^2J_{EX}$	33.7 Hz
$^1J_{EM}$	−291.6 Hz	$^2J_{MX}$	12.2 Hz

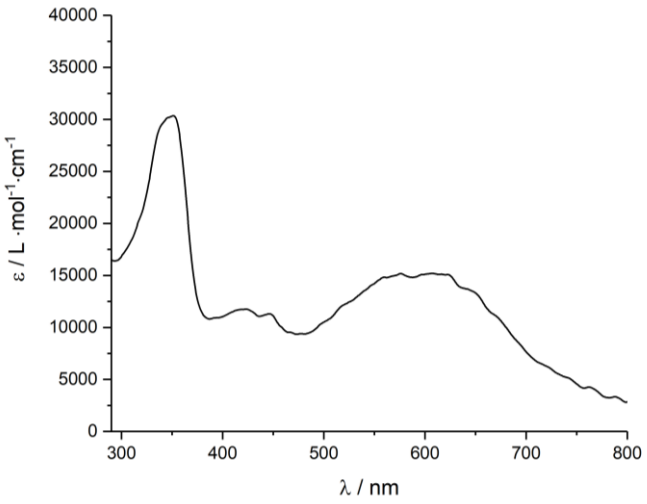

Figure S35. UV/vis spectrum of [(^{Mes}BIAN)Co(μ-η^4:η^1-P$_5$*t*Bu)GaCl(nacnac)] (**5**) recorded in THF.

^{31}P NMR reaction monitoring

In a glovebox 40 mg (0.032 mmol; 1.0 equiv.) [K(dme)$_2${(^{Mes}BIAN)Co(μ-η^4:η^2-P$_4$)Ga(nacnac)}] (**2**) were dissolved in 0.4 mL of THF-d_8 after which 4.85 mg (0.032 mmol; 1.0 equiv.) *i*Pr$_2$PCl in 0.2 mL THF-d_8 was slowly added under stirring. After 5 minutes the reaction mixture was transferred into a J. Young valve NMR tube and the first NMR-measurements started 5 minutes later. ^{1}H, ^{31}P{^{1}H} and ^{31}P and NMR measurements were performed after every hour in the course of six hours. After that the intermediate time was extended to 4 hours and the measurements continued for 102 hours. Throughout the reaction monitoring the NMR tube was kept spinning with 20 Hz to obtain a homogeneous solution.

^{31}P NMR reaction monitoring

In a glovebox 25 mg (0.02 mmol; 1.0 equiv.) [K(dme)$_2${(^{Mes}BIAN)Co(μ-η^4:η^2-P$_4$)Ga(nacnac)}] (**2**) were dissolved in 0.4 mL of THF-d_8 after which 3 mg (0.02 mmol; 1.0 equiv.) *i*Pr$_2$PCl in 0.2 mL THF-d_8 was slowly added while stirring. After 5 minutes the reaction mixture was transferred into a J. Young valve NMR tube and the first NMR-measurements started 5 minutes later. ^{1}H and ^{31}P{^{1}H} NMR measurements were performed in a temperature range from 240 K to 329 K. After every hour the temperature was increased by 10 K. Due to the boiling point of THF (339 K), 329 K was the highest temperature achievable. Throughout the measurement the NMR tube was kept spinning with 20 Hz to obtain a homogeneous solution.

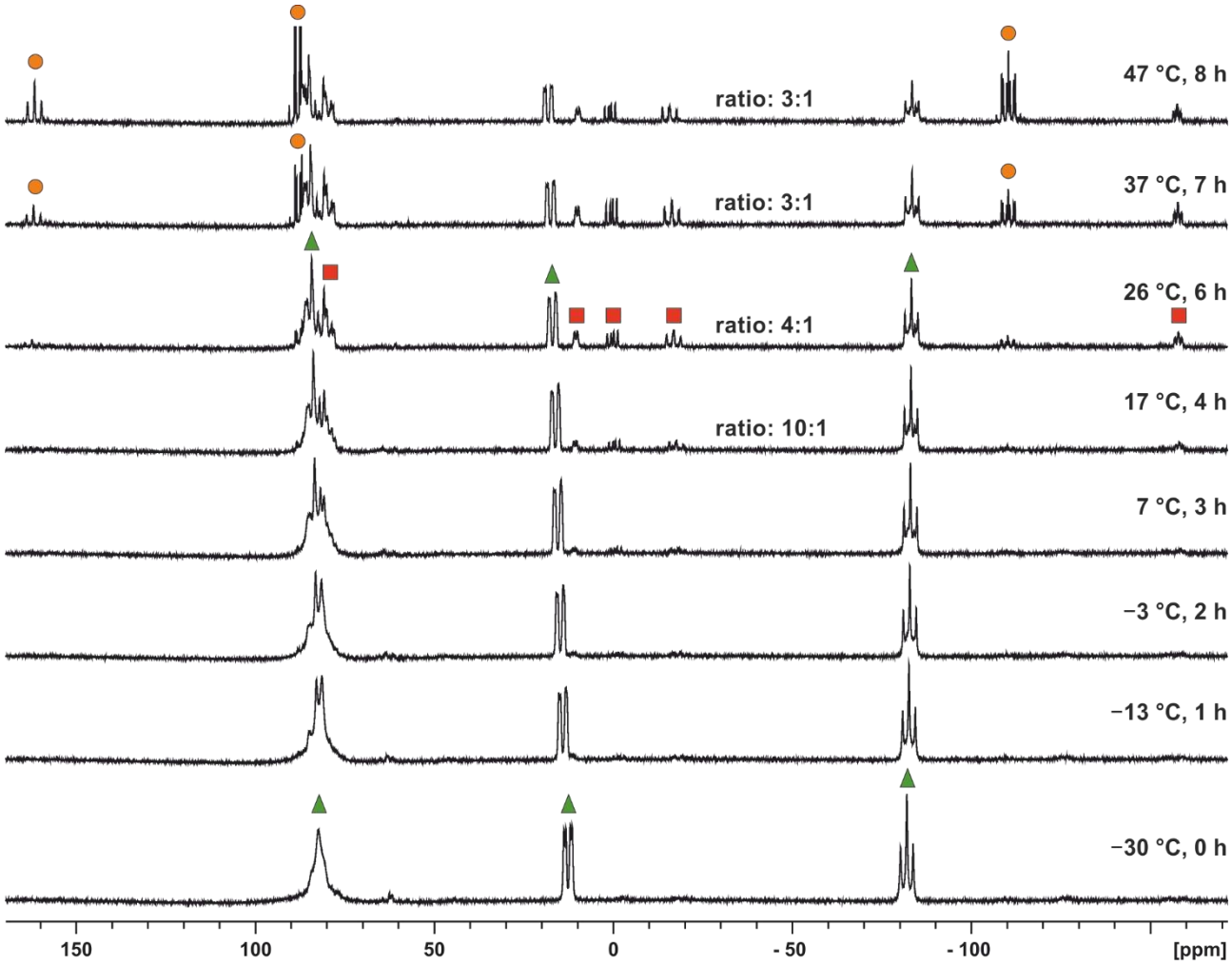

Figure S36. ^{31}P{^{1}H} VT NMR monitoring of the reaction of **2** dissolved in in THF-d_8 with *i*Pr$_2$PCl in a 1:1 ratio; resonances marked with ● are assigned to product [(^{Mes}BIAN)Co(η^4-P$_5$*i*Pr$_2$)] (**3a**) whereas those marked with ▲ (**Int-A**) and ■ (**Int-B**) are assigned to intermediates. The ratio of **Int-A** and **Int-B** was determined by ^{31}P{^{1}H} NMR integration.

X-ray crystallography

The single crystal X-ray diffraction data were recorded on an Agilent Technologies SuperNova in case of **2**, **2'**, **3b**, **3c, 5** and on a GV1000 diffractometer in case of **1**, **3b**, and **4** with Cu Kα radiation (λ = 1.54184 Å). Empirical multi-scan[11] and analytical absorption corrections[12,13] were applied to the data. The structures were solved with SHELXT[14] and least-square refinements on F^2 were carried out with SHELXL[15]. During the refinement of structure **2** the PLATON Squeeze model was applied to one highly disordered molecule DME per formula unit, which was found in a volume of 841.6 Å^3 containing 92.9 electrons.[16] Compound **4** crystallized as multicrystal in the triclinic space group $P\bar{1}$. Three unit cells were identified. For each unit cell a separate data reduction was performed using the multicrystal/twining data reduction tool as implemented in CrysAlisPro.[13] In case of **4·thf** a solvent mask was calculated and 79.5 electrons were found in a volume of 543.0 Å^3. This is consistent with the presence of one molecule THF per formula unit (80 electrons) using Olex Solvent Mask.[17]

CCDC 1861837 (**1-dme**), 1861833 (**2**), 1861832 (**2'**), 1861829 (**3a**), 1861830 (**3b**), 1861831 (**3c**), 1861834 (**4·thf**), 1861835 (**4·*n*-hexane**), 1861836 (**4'·*n*-hexane**), and 1874059 (**5**) contain the supplementary crystallographic data for this paper. These data are provided free of charge by The Cambridge Crystallographic Data Centre.

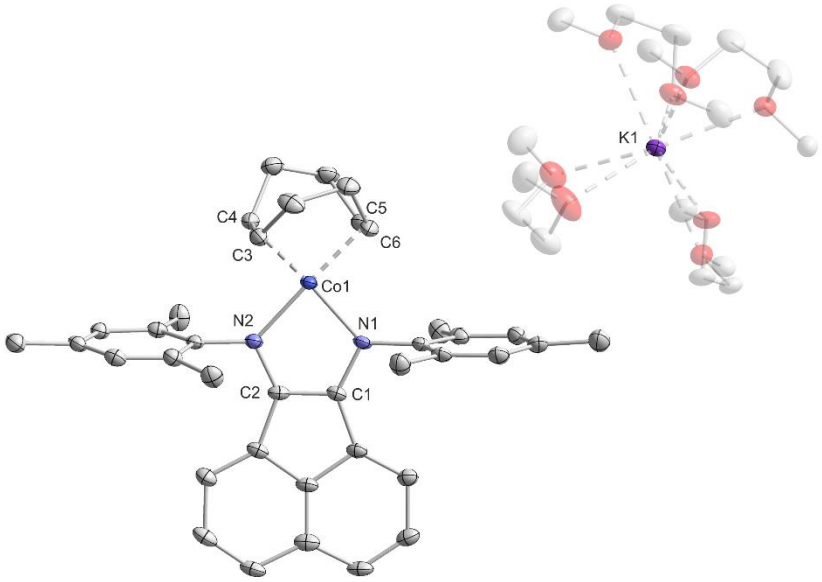

Figure S37. Solid-state molecular structure of [K(dme)$_4${Co(^{Mes}BIAN)(cod)}] (**1-dme**); hydrogen atoms are omitted for clarity and thermal ellipsoids are drawn at the 40% probability level; selected bond lengths [Å] and angles [°]: C1–C2 1.377(5), C1–N1 1.378(5), C2–N2 1.370(4), C3–C4 1.400(6), C5–C6 1.387(6), N1–Co1–N2 84.18(1), bite angle cod-ligand 90.36(3), torsion angle N1–N2–C_{34cent}–C_{56cent} 13.60(2).

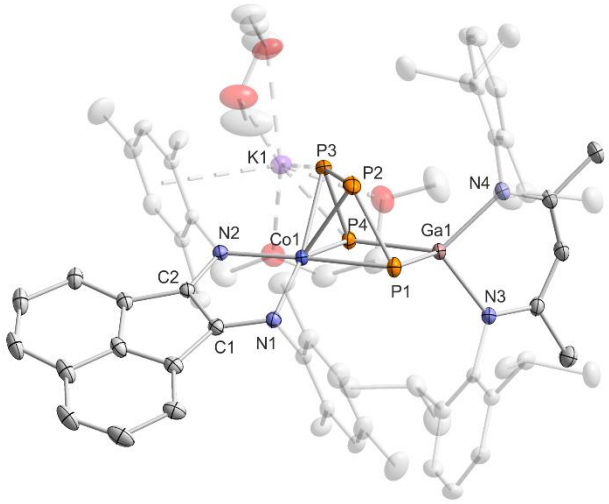

Figure S38. Solid-state molecular structure of [K(dme)$_2${(^{Mes}BIAN)Co(μ-η^4:η^2-P$_4$)Ga(nacnac)}] (**2**); hydrogen atoms are omitted for clarity and thermal ellipsoids are drawn at the 40% probability level; selected bond lengths [Å] and angles [°]: P1–P2 2.1198(7), P2–P3 2.1755(8), P3–P4 2.1286(7), P4–Ga1 2.3328(5), P1…P4 3.3073(6), P1–Ga1 2.3179(5), Ga1–N3 1.991(1), Ga1–N4 2.014(2), Co1–P1 2.3514(6), Co1–P2 2.3098(6), Co1–P3 2.3117(5), Co1–P4 2.3961(6), Co1–N1 1.918(2), Co1–N2 1.948(2), N1–C1 1.337(2), N2–C2 1.334(2), C1–C2 1.411(3), K1–P3 3.7168(7), K1–P4 3.3430(6), Ga1–P4–P3 94.85(2), P4–P3–P2 106.97(3), P3–P2–P1 103.92(3), P2–P1–Ga1 97.31(2), P1–Ga1–P4 90.66(2).

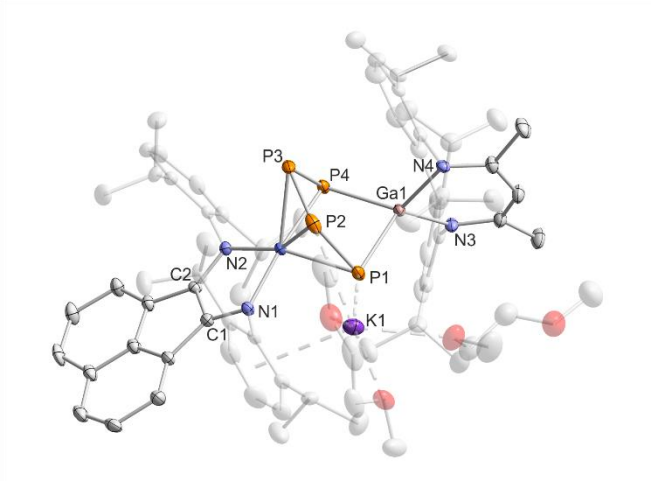

Figure S39. Solid-state molecular structure of [K(dme)$_2${([Dipp]BIAN)Co(μ-η^4:η^2-P$_4$)Ga(nacnac)}] (**2'**); hydrogen atoms are omitted for clarity. Thermal ellipsoids are drawn at the 40% probability level. Selected bond lengths [Å] and angles [°]: P1–P2 2.130(1), P2–P3 2.176(1), P3–P4 2.125(1), P4–Ga1 2.3350(9), P1…P4 3.263(1), P1–Ga1 2.3301(9), Ga1–N3 1.975(3), Ga1–N4 2.015(3), Co1–P1 2.3730(9), Co1–P2 2.3106(9), Co1–P3 2.3105(9), Co1–P4 2.371(1), Co1–N1 1.944(3), Co1–N2 1.940(3), N1–C1 1.336(4), N2–C2 1.338(4), C1–C2 1.406(5), K1–P1 3.393(1), K1–P2 3.548(1), Ga1–P4–P3 96.59(4), P4–P3–P2 103.86(5), P3–P2–P1 105.71(5), P2–P1–Ga1 94.85(4), P1–Ga1–P4 88.75(3).

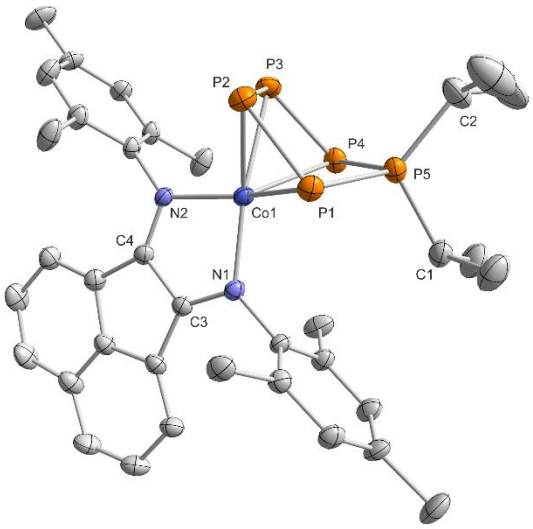

Figure S40. Solid-state molecular structure of [([Mes]BIAN)Co(cyclo-P$_5$*i*Pr$_2$)] (**3a**); hydrogen atoms and solvent molecules are omitted for clarity and thermal ellipsoids are drawn at the 40% probability level; selected bond lengths [Å] and angles [°]: P1–P2 2.12969(2), P2–P3 2.1576(2), P3–P4 2.1297(2), P4–P5 2.1347(2), P5–P1 2.1506(1), P5–C1 1.8423(1), P5–C2 1.8458(1), Co1–P1 2.3720(1), Co1–P2 2.3442(1), Co1–P3 2.3447(2), Co1–P4 2.3595(2), Co1–N1 1.9104(1), Co1–N2 1.9480(1), N1–C3 1.32559(8), N2–C4 1.32069(8), C3–C4 1.4366(1), P1–P2–P3 103.926(5), P2–P3–P4 107.049(5), P3–P4–P5 98.104(6), P4–P5–P1 99.966(5), P5–P1–P2 100.689(5), C1–P5–C2 113.0644(5).

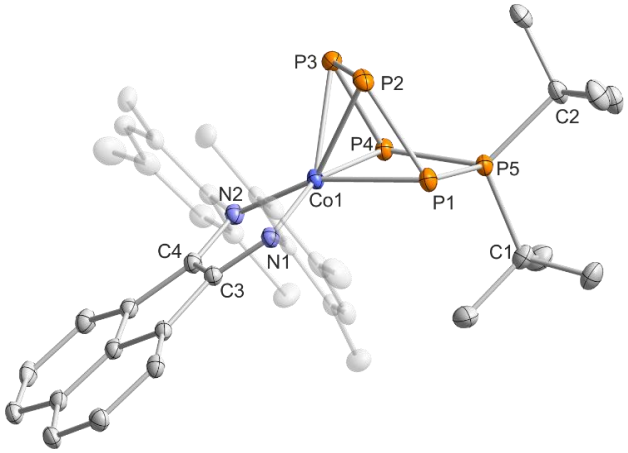

Figure S41. Solid-state molecular structure of [([Mes]BIAN)Co(cyclo-P$_5$*t*Bu$_2$)] (**3b**); hydrogen atoms and solvent molecules are omitted for clarity and thermal ellipsoids are drawn at the 40% probability level. Selected bond lengths [Å] and angles [°]: P1–P2 2.1572(8), P2–P3 2.1310(9), P3–P4 2.1641(9), P5–P1 2.1634(8), P4–P5 2.1626(8), P5–C1 1.888(3), P5–C2 1.897(3), Co1–P1 2.3327(7), Co1–P2 2.3251(7), Co1–P3 2.3211(7), Co1–P4 2.3459(7), Co1–N1 1.925(2), Co1–N2 1.924(2), N1–C3 1.336(3), N2–C4 1.325(3), C3–C4 1.414(3), P1–P2–P3 103.61(3), P2–P3–P4 104.44(3), P3–P4–P5 100.66(3), P4–P5–P1 94.58(3), P5–P4–P3 101.93(3), C1–P5–C2 111.4(1).

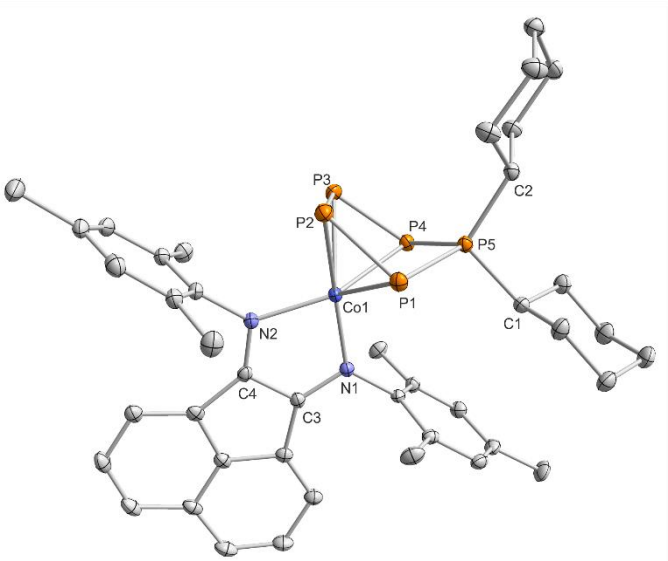

Figure S42. Solid-state molecular structure of [(^{Mes}BIAN)Co(cyclo-P_5Cy_2)] (**3c**) hydrogen atoms and solvent molecules are omitted for clarity thermal ellipsoids are drawn at the 40% probability level; Selected bond lengths [Å] and angles [°]: P1–P2 2.1246(1), P2–P3 2.1566(1), P3–P4 2.1285(2), P4–P5 2.1504(1), P5–P1 2.1561(2), P5–C1 1.8412(1), P5–C2 1.85192(9), Co1–P1 2.3473(1), Co1–P2 2.3385(1), Co1–P3 2.33926(9), Co1–P4 2.3704(2), Co1–N1 1.90439(8), Co1–N2 1.9378(1), N1–C3 1.33410(8), N2–C4 1.32937(5), C3–C4 1.41812(8), P1–P2–P3 104.116(5), P2–P3–P4 106.735(5), P3–P4–P5 97.747(5), P4–P5–P1 99.554(5), P5–P1–P2 99.783(5), C1–P5–C2 106.874(4).

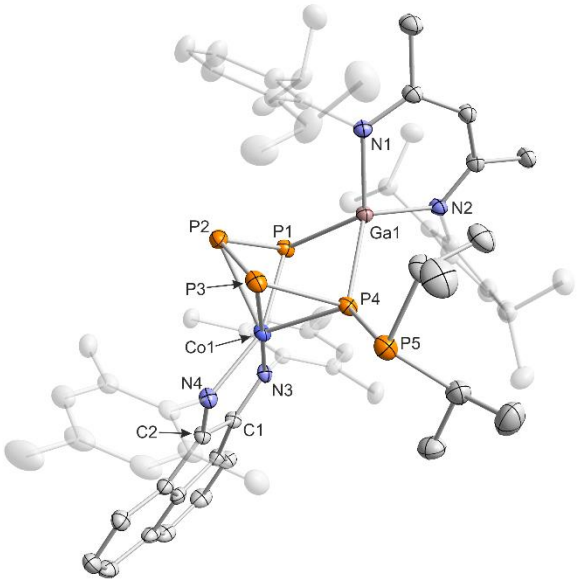

Figure S43. Solid-state molecular structure of [(^{Mes}BIAN)Co(μ-η^4:η^2-P_5iPr_2)Ga(nacnac)}] (**4**) hydrogen atoms are omitted for clarity thermal ellipsoids are drawn at the 40% probability level; selected bond lengths [Å] and angles [°]: P1–P2 2.122(1), P2–P3 2.159(2), P3–P4 2.164(1), P4–P5 2.239(1), P1–Ga1 2.3320(9), P4–Ga1 2.418(1), Ga1–N1 1.992(3), Ga1–N2 1.974(3), Co1–P1 2.348(2), Co1–P2 2.37(1), Co1–P3 2.306(1), Co1–P4 2.353(1), Co1–N3 1.919(3), Co1-N4 1.963(3), C1–N3 1.335(4), C2–N4 1.323(4), C1–C2 1.422(5), P1–P2–P3 103.59(5), P2–P3–P4 102.46(5), P3–P4–P5 93.59(5), P5–P4–Ga1 133.22(5), P4–Ga1–P1 82.28(3), Ga1–P1–P2 97.13(4).

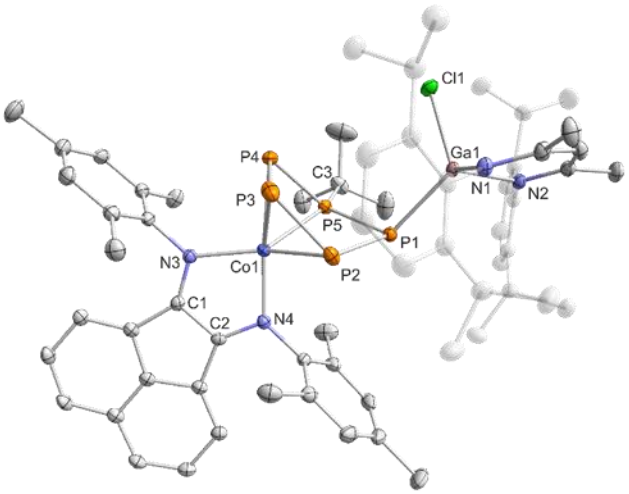

Figure S44. Solid-state molecular structure of [(MesBIAN)Co(μ-η^4:η^1-P$_5$*t*Bu)GaCl(nacnac)] (**5**); hydrogen atoms are omitted for clarity and thermal ellipsoids are drawn at the 40% probability level; selected bond lengths [Å] and angles [°]: P1–P2 2.19903(6), P2–P3 2.14129(5), P3–P4 2.13102(7), P4–P5 2.13310(5), P5–P1 2.14148(6), P1–Ga1 2.34200(6), P5–C3 1.89094(6), Ga1–N1 1.94202(6), Ga1–N2 1.96271(5), Ga1–Cl1 2.20080(5), Co1–P2 2.33156(7), Co1–P3 2.33788(6), Co1–P4 2.37439(6), Co1–P5 2.23375(6), Co1–N3 1.95761(5), Co1–N4 1.90519(4), C1–N3 1.31832(3), C2–N4 1.32622(3), C1–C2 1.42740(3); P1–P2–P3 113.062(2), P2–P3–P4 103.661(2), P3–P4–P5 97.566(2), P4–P5–P1 118.046(2), P5–P1–P2 84.471(2), P4–P5–C3 112.065(2), P4–P5–C3 115.399(2), Ga1–P1–P5 115.834(2), Ga1–P1–P2 112.634(2).

Table S7. Crystallographic data of **1**, **2** and **2'**.

Compound	**1a**	**2**	**2'**
Empirical formula	$C_{54}H_{80}CoKN_2O_8$	$C_{67}H_{89}CoGaKN_4O_4P_4$	$C_{77}H_{111}CoGaKN_4O_6P_4$
Formula weight	983.23	1306.05	1480.32
Temperature [K]	123(1)	123(1)	123(1)
Crystal system	triclinic	triclinic	orthorhombic
Space group	*P*-1	*P*-1	$P2_12_12_1$
a [Å]	15.3646(3)	15.4512(3)	13.84854(12)
b [Å]	25.7695(5)	16.1163(4)	21.0014(2)
c [Å]	27.6375(4)	16.5636(3)	27.3815(3)
α [°]	105.4393(15)	94.7947(16)	90
β [°]	90.5348(15)	103.1479(16)	90
γ [°]	90.8565(17)	98.1715(18)	90
Volume [Å^3]	10545.7(4)	3946.83(14)	7963.62(13)
Z	8	2	4
ρ_{calc} [g/cm^3]	1.239	1.099	1.235
μ [mm^{-1}]	3.678	3.623	3.668
F(000)	4224.0	1376.0	3144.0
Crystal size [mm^3]	0.1887 × 0.132 × 0.0838	0.3316 × 0.1837 × 0.1439	0.227 × 0.205 × 0.125
Radiation	CuKα (λ = 1.54184)	CuKα (λ = 1.54184)	CuKα (λ = 1.54184)
2Θ range for data collection [°]	6.642 to 147.204	7.072 to 153.024	7.154 to 147.026
Index ranges	-19 ≤ h ≤ 18, -31 ≤ k ≤ 31, -33 ≤ l ≤ 34	-19 ≤ h ≤ 19, -18 ≤ k ≤ 20, -20 ≤ l ≤ 20	-12 ≤ h ≤ 17, -25 ≤ k ≤ 18, -34 ≤ l ≤ 33
Reflections collected	135248	50128	37068
Independent reflections	41065 [R_{int} = 0.0703, R_{sigma} = 0.0655]	16206 [R_{int} = 0.0288, R_{sigma} = 0.0273]	14919 [R_{int} = 0.0347, R_{sigma} = 0.0376]
Data / restraints / parameters	41065/0/2479	16206/0/759	14919/167/936
Goodness-of-fit on F^2	1.010	1.036	1.093
Final R indexes [I>=2σ (I)]	R_1 = 0.0710, wR_2 = 0.1778	R_1 = 0.0380, wR_2 = 0.1075	R_1 = 0.0343, wR_2 = 0.0979
Final R indexes [all data]	R_1 = 0.0997, wR_2 = 0.1999	R_1 = 0.0395, wR_2 = 0.1089	R_1 = 0.0387, wR_2 = 0.1081
Largest diff. peak/hole [e Å^{-3}]	1.54/-0.68	0.89/-0.51	0.53/-0.65
Flack parameter	-	-	-0.0292(17)

Table S8. Crystallographic data of 3a-c.

Compound	**3a**	**3b**	**3c**
Empirical formula	$C_{39}H_{49}CoN_2P_5$	$C_{41}H_{53}CoN_2P_5$	$C_{45}H_{57}CoN_2P_5$
Formula weight	759.58	787.63	839.70
Temperature [K]	123(1))	123(1)	123(1)
Crystal system	triclinic	triclinic	triclinic
Space group	*P*-1	*P*-1	*P*-1
a [Å]	8.2950(6)	11.5086(6)	11.0975(4)
b [Å]	10.3193(6)	12.6623(6)	12.9085(8)
c [Å]	23.1847(14)	16.1055(8)	16.7384(9)
α [°]	84.114(5)	71.013(4)	68.191(5)
β [°]	82.677(5)	69.473(5)	88.775(4)
γ [°]	80.838(6)	70.661(4)	72.802(4)
Volume [Å^3]	1936.4(2)	2015.0(2)	2116.1(2)
Z	2	2	2
ρ_{calc} [g/cm^3]	1.303	1.298	1.318
μ [mm^{-1}]	5.648	5.446	5.220
F(000)	798.0	830.0	886.0
Crystal size [mm^3]	0.374 × 0.092 × 0.037	0.36 × 0.19 × 0.158	0.167 × 0.074 × 0.046
Radiation	CuKα (λ = 1.54184)	CuKα (λ = 1.54184)	CuKα (λ = 1.54184)
2Θ range for data collection [°]	7.716 to 147.388	7.616 to 148.178	7.678 to 148.1
Index ranges	-9 ≤ h ≤ 10, -12 ≤ k ≤ 11, -27 ≤ l ≤ 28	-13 ≤ h ≤ 14, -15 ≤ k ≤ 15, -19 ≤ l ≤ 20	-13 ≤ h ≤ 11, -15 ≤ k ≤ 14, -20 ≤ l ≤ 20
Reflections collected	11921	13999	19056
Independent reflections	7390 [R_{int} = 0.0460, R_{sigma} = 0.0627]	7873 [R_{int} = 0.0457, R_{sigma} = 0.0477]	8231 [R_{int} = 0.0397, R_{sigma} = 0.0543]
Data / restraints / parameters	7390/30/421	7873/0/455	8231/0/485
Goodness-of-fit on F^2	1.018	1.026	1.085
Final R indexes [I>=2σ (I)]	R_1 = 0.0793, wR_2 = 0.2044	R_1 = 0.0544, wR_2 = 0.1467	R_1 = 0.0492, wR_2 = 0.1123
Final R indexes [all data]	R_1 = 0.0902, wR_2 = 0.2164	R_1 = 0.0563, wR_2 = 0.1501	R_1 = 0.0601, wR_2 = 0.1164
Largest diff. peak/hole [e Å^{-3}]	2.01/-0.88	1.02/-0.70	0.56/-0.38

Table S9. Crystallographic data of multicrystal 4.

Compound	**4 · thf**	**4 · *n*-hexane**	**4 · *n*-hexane**
Empirical formula	$C_{69}H_{90}CoGaN_4OP_5$	$C_{68}H_{90}CoGaN_4P_5$	$C_{68}H_{90}CoGaN_4P_5$
Formula weight	1274.21	1246.93	1246.93
Temperature [K]	123(1)	123(1)	123(1)
Crystal system	triclinic	triclinic	triclinic
Space group	*P*-1	*P*-1	*P*-1
a [Å]	12.5761(4)	12.0763(7)	12.0909(7)
b [Å]	16.9742(4)	12.7169(7)	12.7157(7)
c [Å]	17.4872(4)	21.8615(9)	21.8419(9)
α [°]	97.670(2)	99.614(4)	99.628(4)
β [°]	101.165(2)	94.655(4)	94.661(4)
γ [°]	94.952(2)	102.639(4)	102.632(5)
Volume [Å^3]	3605.33(17)	3205.7(3)	3206.3(3)
Z	2	2	2
ρ_{calc} [g/cm^3]	1.174	1.292	1.292
μ [mm^{-1}]	3.620	4.046	4.045
F(000)	1345.0	1318.0	1318.0
Crystal size [mm^3]	0.333 × 0.212 × 0.155	0.333 × 0.212 × 0.155	0.333 × 0.212 × 0.155
Radiation	CuKα (λ = 1.54184)	CuKα (λ = 1.54184)	CuKα (λ = 1.54184)
2Θ range for data collection [°]	7.212 to 147.944	7.256 to 147.88	7.258 to 147.586
Index ranges	-14 ≤ h ≤ 15, -15 ≤ k ≤ 20, -16 ≤ l ≤ 21	-13 ≤ h ≤ 14, -11 ≤ k ≤ 15, -26 ≤ l ≤ 20	-14 ≤ h ≤ 14, -11 ≤ k ≤ 15, -26 ≤ l ≤ 20
Reflections collected	21456	18878	19055
Independent reflections	13684 [R_{int} = 0.0558, R_{sigma} = 0.0463]	11950 [R_{int} = 0.0629, R_{sigma} = 0.0683]	12115 [R_{int} = 0.0739, R_{sigma} = 0.0779]
Data / restraints / parameters	13684/13/733	11950/0/733	12115/0/733
Goodness-of-fit on F^2	1.050	1.040	1.039
Final R indexes [I>=2σ (I)]	R_1 = 0.0647, wR_2 = 0.1799	R_1 = 0.0717, wR_2 = 0.1887	R_1 = 0.0802, wR_2 = 0.2163
Final R indexes [all data]	R1 = 0.0667, wR2 = 0.1832	R_1 = 0.0804, wR_2 = 0.2019	R_1 = 0.0900, wR_2 = 0.2322
Largest diff. peak/hole [e Å^{-3}]	1.64/-1.35	1.16/-1.44	1.53/-1.29

Table S10. Crystallographic data of 5.

Compound	**5**
Empirical formula	$C_{75}H_{88}ClCoF_2GaN_4P_5$
Formula weight	1402.44
Temperature [K]	123 (1)
Crystal system	triclinic
Space group	*P*-1
a [Å]	11.8741(3)
b [Å]	12.4783(3)
c [Å]	24.9702(6)
α [°]	89.008(2)
β [°]	77.087(2)
γ [°]	78.673(2)
Volume [Å^3]	3534.63(15)
Z	2
ρ_{calc} [g/cm^3]	1.318
μ [mm^{-1}]	4.115
F(000)	1468.0
Crystal size [mm^3]	0.402 × 0.36 × 0.197
Radiation	CuKα (λ = 1.54184)
2Θ range for data collection [°]	7.228 to 148.414
Index ranges	-14 ≤ h ≤ 14, -15 ≤ k ≤ 15, -31 ≤ l ≤ 29
Reflections collected	28770
Independent reflections	13997 [R_{int} = 0.0329, R_{sigma} = 0.0378]
Data / restraints / parameters	13997/0/831
Goodness-of-fit on F^2	1.037
Final R indexes [I>=2σ (I)]	R_1 = 0.0444, wR_2 = 0.1162
Final R indexes [all data]	R_1 = 0.0461, wR_2 = 0.1179
Largest diff. peak/hole [e Å^{-3}]	1.85/-0.60

Computational Details

Geometry optimization and electronic structure of a truncated model compound

Prior to the calculation of the phosphorus chemical shielding σ_{calcd} the electronic structure of the compounds **2**, **3b** and **4** was analyzed with respect to the redox active BIAN ligand. Benchmark studies were performed on a truncated model complex **3'** (Figure S45) using the Gaussian09 program package (Revision E.01).[18]

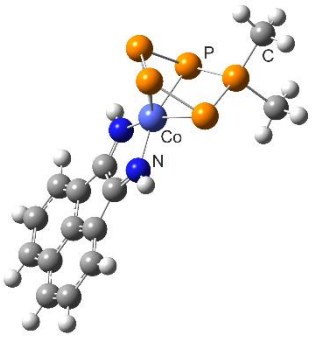

Figure S45. Representation of the truncated model complex **3'**.

The geometry of **3'** was optimized in the closed-shell singlet configuration on the B3LYP/6-311G(d) level of theory. Subsequently, single point calculations were performed on different possible electronic configurations (Table S9).

Table S11. DFT computed single point energies of different electronic configurations of **3'** on the B3LYP/6-311G(d) level of theory.

	closed-shell singlet (S = 0)	open-shell singlet (S = 0)	triplet (S =1)
Energy (hartree)	−3741.270596	−3741.271997	−3741.246415
S^2	0.00	0.6072	2.0353
ΔE (kcal/mol)	0.00	-0.88	15.17

The preliminary benchmark studies revealed that the triplet (S = 1) state is less favored (15.17 kcal/mol) relative to the closed-shell configuration (S = 0). The relative energies of the open-shell singlet configuration to the closed-shell system are close together and differ only by 0.88 kcal/mol, suggesting an open-shell spin state. The single-reference broken symmetry approach only yields an approximate solution, in which an antiferromagnetic coupling between an unpaired electron of the BIAN ligand with an unpaired electron of the cobalt atom is observed (Figure S46). However, DFT is a single reference method and relative energies of species in different spin state configurations are innately troublesome. Due to the very small energy difference of open-shell to closed-shell configuration (0.88 kcal/mol) the true electronic structure of model complex **3'** cannot be sufficiently described using standard DFT methods.[19–23]

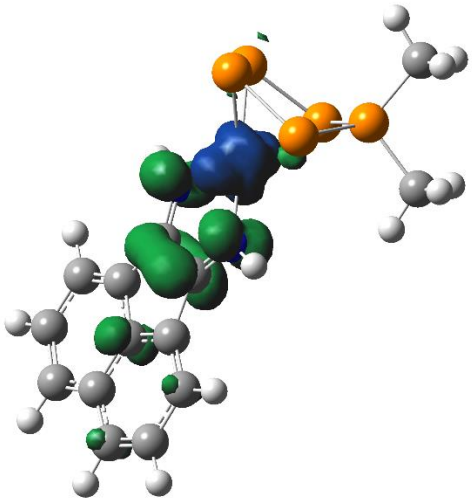

Figure S46. Spin density plot of the open-shell singlet state calculated at the uB3LYP/6-311G(d) level of theory (Isosurface value 0.004). Mulliken spin densities: Co 0.83, BIAN −0.64.

Multi-reference approaches, such as CASSCF, are able to accurately describe the electronic structure of open-shell singlet configurations. However, such large systems present in compounds **2**, **3a** and **4** are currently too expensive to optimize with these multi-reference methods.[19–23]
Thus, we decided to optimize the full systems **2**, **3a** and **4** in a closed-shell singlet configuration, well knowing that the obtained electronic state is only an approximation. The meta-hybrid functional TPSSh together with split basis sets (def2-QZVP for Co, N, P, Ga; and def2-SVP for C, H) were employed. The optimized structures are in good agreement with the single crystal X-ray diffraction measurements and the nature of the stationary points was further verified by numerical frequency analyses.

Calculation of ^{31}P NMR chemical shielding

Even though the closed shell configuration of compounds **2**, **3a** and **4** does not represent the true electronic structure we calculated the phosphorus chemical shielding σ_{calcd} using the Amsterdam Density Functional program package.[24] The pre-optimized structures were supplied to ADF, optimized at the PBE-D3BJ/TZP level of theory and subsequently supplied to ADF's EPR/NMR program to calculate the ^{31}P chemical shielding. The obtained values are calculated relative to a bare phosphorus nucleus. They can be converted to chemical shifts δ relative to an appropriate reference system for which we used the ^{31}P NMR reference compound 85% aqueous phosphoric acid as not stated otherwise. Complex **3a** has shown to be an inappropriate reference system for the Ga containing complexes **2** and **4**.

The theoretical magnetic shielding of 85% aqueous H_3PO_4 can hardly be obtained and auxiliary substances for which gas-phase NMR data are available have to be used (PH_3 δ_g = 266.1 ppm). The calculated phosphorus chemical shielding σ_{calcd} can be converted into chemical shifts by this relationship:[25]

$$\delta(s,calc) = \sigma(PH_3, calc) - \sigma(s, calc) - 266.1 \text{ ppm}$$

$\sigma(PH_3, calc)$ is the theoretical magnetic shielding of PH_3 calculated at the PBE-D3BJ/TZP level of theory using ADF (σ_{calcd} = 584.9).

*^{31}P NMR chemical shielding of **3a***

At first, the phosphorus chemical shieldings σ_{calcd} for **3a** were calculated to show that the ^{31}P chemical shielding in the closed-shell configurations give the same trend as those observed experimentally (Table S10). The experimental ^{31}P NMR spectrum of **3a** displays a symmetric splitting pattern in solution. Thus, the geometry of **3a** was optimized once in a C_s constrained symmetry and once without any symmetry constraint. The resulting C_s symmetric complex **3a^{Cs}** is about 1 kcal/mol less favored to the unsymmetrical geometry resemble the XRD data.

Table S12. PBE-D3BJ/TZP ^{31}P NMR chemical shieldings σ_{calcd} and chemical shifts δ_{calcd} [ppm] of complex **3a** and the C_s symmetry constrained complex **3a^{Cs}**; [Co] = (^{Mes}BIAN)Co.

	3a		**3a^{Cs}**		**Experimental Values**
	σ_{calcd}	δ_{calcd}	σ_{calcd}	δ_{calcd}	δ_{exp}
P(5) MM'	243.27	75.5	222.3	96.5	88.6
P(4) MM'	202.79	116.0	222.4	96.4	88.6
P(3) XX'	458.34	−139.6	467.3	−148.5	−111.4
P(2) XX'	464.82	−146.0	467.3	−148.5	−111.4
P(1) A	143.00	175.8	137.7	181.1	161

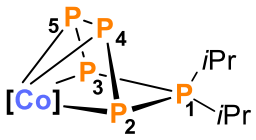

By comparing the theoretical values with the experimental ones, we conclude, that the ^{31}P NMR calculated chemical shifts represent the right trend and can be employed to further investigate compounds **2** and **4**.

*^{31}P NMR chemical shielding of **4***

The calculated chemical ^{31}P NMR chemical shieldings σ_{calcd} and chemical shifts δ_{calcd} for compound **4** are given in Table S11. Chemical shifts were referenced either to 85% aqueous phosphoric acid or were referenced internally to phosphorus atom P2.

Table S13. PBE-D3BJ/TZP ^{31}P NMR chemical shieldings σ_{calcd} and chemical shifts δ_{calcd} [ppm] of complex **4**; [Co] = (^{Mes}BIAN)Co; [Ga] = (nacnac)Ga.

	4			**Experimental Values**
	σ_{calcd}	δ_{calcd}[a]	δ_{calcd} [b]	δ_{exp}
P(1)	273.5	45.2	21.6	15.0
P(2)	378.2	−59.4	-83.0	−83.0
P(3)	202.2	116.6	93.0	88.1
P(4)	198.8	120.0	96.4	88.1
P(5)	187.6	131.2	107.6	81.1

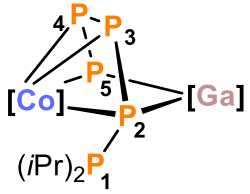

[a] Referenced to 85% aqueous phosphoric acid; [b] P2 used as reference chemical shift (δ_{ref} = 295.2 ppm)

The theoretically obtained phosphorus chemical shifts resemble a similar trend like it is observed for intermediate **Int-1** in the ^{31}P NMR reaction monitoring experiment (Figure S47). Thus, we conclude, that the phosphorus chemical shifts of intermediate **Int-1** are likely assigned to compound **4**.

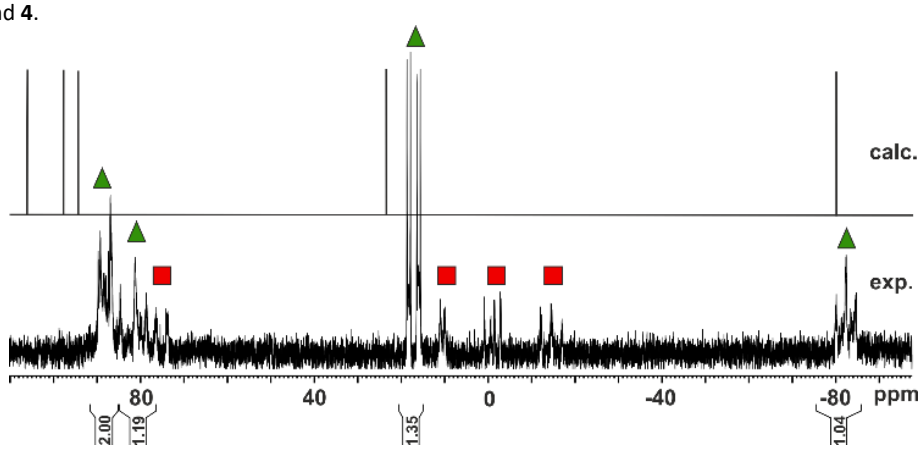

Figure S47. Section of ^{31}P{^{1}H} NMR spectrum of crystalline **4** in C_6D_6; resonances marked with ▲ (**Int-1**) and ■ (**Int-2**) are assigned to the intermediates (bottom); calculated ^{31}P NMR chemical shifts of **4** referenced internally to P2 (top).

*^{31}P NMR chemical shielding of **2***

In order to properly assign the P-atoms in compounds **2** and **2'** the ^{31}P NMR chemical shieldings of anion **2** were calculated. The trend of calculated and experimental chemical shifts were compared and the high-field shifted signal can clearly be assigned to the Ga-bound phosphorus atoms.

Table S14. PBE-D3BJ/TZP ^{31}P NMR chemical shieldings σ_{calcd} and chemical shifts δ_{calcd} [ppm] of anion **2'**; [Co] = ^{Mes}BIAN)Co; [Ga] = (nacnac)Ga.

	2		**Experimental Values**
	σ_{calcd}	δ_{calcd}	δ_{exp}
P(1) XX'	417.4	−98.6	−125.4
P(4) XX'	418.5	−99.7	−125.4
P(2) AA'	194.6	124.2	74.0
P(3) AA'	243.0	75.8	74.0

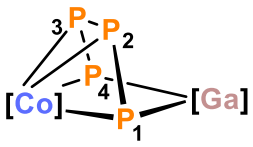

References

References

1 P. H. M. Budzelaar, *gNMR for Windows (5.0.6.0), NMR Simulation Programm*, 2006.
2 a) S. Aime, R. K. Harris, E. M. McVicker and M. Fild, *J. Chem. Soc., Dalton Trans.*, 1976, 2144; b) H. C. E. McFarlane, W. McFarlane and J. A. Nash, *J. Chem. Soc., Dalton Trans.*, 1980, 240; c) J. P. Albrand, H. Faucher, D. Gagnaire and J. B. Robert, *Chem. Phys. Lett.*, 1976, **38**, 521; d) J. E. Del Bene, J. Elguero and I. Alkorta, *J. Phys. Chem. A*, 2004, **108**, 3662; e) E. G. Finer and R. K. Harris, *Mol. Phys.*, 1967, **13**, 65; f) M. A. M. Forgeron, M. Gee and R. E. Wasylishen, *J. Phys. Chem. A*, 2004, **108**, 4895;
3 R. K. Harris, E. D. Becker, S. M. Cabral de Menezes, R. Goodfellow and P. Granger, *Magn. Reson. Chem.*, 2002, **40**, 489.
4 a) K. Jonas, R. Mynott, C. Krüger, J. C. Sekutowski and Y.-H. Tsay, *Angew. Chem. Int. Ed. Engl.*, 1976, **15**, 767; b) [Der Titel "K. Jonas, US patent 4169845, 1979. – Method of preparing transition metal-olefin" kann nicht dargestellt werden. Die Vorlage "Literaturverzeichnis - Patentschrift - (Standardvorlage)" beinhaltet nur Felder, welche bei diesem Titel leer sind.];
5 S. Pelties, T. Maier, D. Herrmann, B. d. Bruin, C. Rebreyend, S. Gärtner, I. G. Shenderovich and R. Wolf, *Chem. Eur. J.*, 2017, **23**, 6094.
6 G. Prabusankar, A. Doddi, C. Gemel, M. Winter and R. A. Fischer, *Inorg. Chem.*, 2010, **49**, 7976.
7 M. Gasperini, F. Ragaini and S. Cenini, *Organometallics*, 2002, **21**, 2950.
8 P. Li, B. Lü, C. Fu and S. Ma, *Adv. Synth. Catal.*, 2013, **355**, 1255.
9 a) A. A. Naiini, Y. Han, M. Akinc and J. G. Verkade, *Inorg. Chem.*, 1993, **32**, 5394; b) M. Fild, O. Stelzer, R. Schmutzler and G. O. Doak, *Inorg. Synth.*, 1973, **14**, 4;
10 Y. Liu, B. Ding, D. Liu, Z. Zhang, Y. Liu and W. Zhang, *Res. Chem. Intermed.*, 2017, **43**, 4959.
11 a) SCALE3ABS, CrysAlisPro, Aglient Technologies Inc. Oxford and GB, 2015; b) G. M. Sheldrick, SADABS, Bruker AXS, Madison and USA, 2007;
12 R. C. Clark, J. S. Reid, *Acta Crystallogr. A*, 1995, **51**, 887.
13 CrysAlisPro, version 171.39.37b, Agilent Technologies Inc., Oxford and GB, 2017.
14 G. M. Sheldrick, *Acta Cryst.*, 2015, **A17**, 3.
15 G. M. Sheldrick, *Acta Cryst.*, 2015, **C71**, 3.
16 A. L. Spek, *Acta Cryst.*, 2009, **D65**, 148.
17 O. V. Dolomanov, L. J. Bourhis, R. J. Gildea, J. A. K. Howard and H. Puschmann, *J. Appl. Cryst.*, 2009, **42**, 339.
18 Gaussian 09, Revision E.01, M. J. Frisch, G. W. Trucks, H. B. Schlegel, G. E. Scuseria, M. A. Robb, J. R. Cheeseman, G. Scalmani, V. Barone, G. A. Petersson, H. Nakatsuji, X. Li, M. Caricato, A. Marenich, J. Bloino, B. G. Janesko, R. Gomperts, B. Mennucci, H. P. Hratchian, J. V. Ortiz, A. F. Izmaylov, J. L. Sonnenberg, D. Williams-Young, F. Ding, F. Lipparini, F. Egidi, J. Goings, B. Peng, A. Petrone, T. Henderson, D. Ranasinghe, V. G. Zakrzewski, J. Gao, N. Rega, G. Zheng, W. Liang, M. Hada, M. Ehara, K. Toyota, R. Fukuda, J. Hasegawa, M. Ishida, T. Nakajima, Y. Honda, O. Kitao, H. Nakai, T. Vreven, K. Throssell, J. A. Montgomery, Jr., J. E. Peralta, F. Ogliaro, M. Bearpark, J. J. Heyd, E. Brothers, K. N. Kudin, V. N. Staroverov, T. Keith, R. Kobayashi, J. Normand, K. Raghavachari, A. Rendell, J. C. Burant, S. S. Iyengar, J. Tomasi, M. Cossi, J. M. Millam, M. Klene, C. Adamo, R. Cammi, J. W. Ochterski, R. L. Martin, K. Morokuma, O. Farkas, J. B. Foresman, and D. J. Fox, *Gaussian, Inc., Wallingford CT*, 2009.
19 P. Milko and M. A. Iron, *J. Chem. Theory Comput.*, 2014, **10**, 220.
20 T. Zell, P. Milko, K. L. Fillman, Y. Diskin-Posner, T. Bendikov, M. A. Iron, G. Leitus, Y. Ben-David, M. L. Neidig and D. Milstein, *Chem. Eur. J.*, 2014, **20**, 4403.
21 S. C. Bart, K. Chłopek, E. Bill, M. W. Bouwkamp, E. Lobkovsky, F. Neese, K. Wieghardt and P. J. Chirik, *J. Am. Chem. Soc.*, 2006, **128**, 13901.
22 P. H. M. Budzelaar, B. d. Bruin, A. W. Gal, K. Wieghardt and J. H. van Lenthe, *Inorg. Chem.*, 2001, **40**, 4649.
23 C. Lichtenberg, M. Adelhardt, T. L. Gianetti, K. Meyer, B. d. Bruin and H. Grützmacher, *ACS Catal.*, 2015, **5**, 6230.
24 a) ADF 2017, SCM, Theoretical Chemistry, Vrije Universiteit, Amsterdam, The Netherlands, *http://www.scm.com*; b) C. Fonseca Guerra, J. G. Snijders, G. te Velde and E. J. Baerends, *Theor. Chem. Acc.*, 1998, **99**, 391; c) G. te Velde, F. M. Bickelhaupt, E. J. Baerends, C. Fonseca Guerra, S. J. A. van Gisbergen, J. G. Snijders and T. Ziegler, *J. Comput. Chem.*, 2001, **22**, 931;
25 a) C. van Wüllen, *Phys. Chem. Chem. Phys.*, 2000, **2**, 2137; b) C. J. Jameson, A. de Dios and A. Keith Jameson, *Chemical Physics Letters*, 1990, **167**, 575;